UNIVERSITY OF CALIFORNIA
RIVERSIDE

Chemical Biology Applications of Monocyclic Peptides

A Dissertation submitted in partial satisfaction
of the requirements for the degree of

Doctor of Philosophy

in

Environmental Toxicology

by

Siwen Wang

September 2021

Dissertation Committee:
Dr. Min Xue, Chairperson
Dr. Wenwan Zhong
Dr. Jason Cheng

The Dissertation of Siwen Wang is approved:

Committee Chairperson

University of California, Riverside

Acknowledgments

The work described in this dissertation would not have been possible without guidance from many people. First, I am fully grateful to my supervisor, Dr. Min Xue. Min is always an inspiration to me, I am constantly motivated by and admire his creativity, hard work and dedication to science. I am thankful for the funding, patience and intellectual guidance he has provided me. Thank you to the rest of my committee members: Dr. Wenwan Zhong and Dr. Jason Cheng. It has been a great hour to work with such a distinguished group of scientists.

Importantly, I want to thank my parents for always being there whenever I feel depressed or struggled. I want to thank my mom for being the cheer leader of my entire life. She taught me unconditional love. I also want to express my special thanks to Jennifer Ball for her kindness. Jennifer was my English teacher back in college, she always believed in my potential, encouraged me throughout the whole eight years of our friendship. These two strong, hardworking and beautiful women are my role models. I have experienced a very tough period in my third year while studying at US. I cannot imagine where I would be ended up with without both of their love and support.

In addition, I want to thank other loved ones who are always a constant source of support. Thanks to my lab mate, Priyanka Sarkar, and my roommate, Han Qu and my dear friend Rachel Behar who have helped me developed into the person I am today. You ladies have brought so much joy and positive energy into my life.

Finally, I want to thank Farid Azhir and all the ETOX staff who have worked with me over the years to help improve the quality of life at UCR. My life could not be more enriched without every single one of you.

The text in this dissertation is a reprint of the following publication:

Chapter 3: Wang, S. *et al.* Digitonin-facilitated delivery of imaging probes enables single-cell analysis of AKT signalling activities in suspension cells. *The Analyst* (2021).

Dedication

To my dear parents and Jennifer

ABSTRACT OF THE DISSERTATION

Chemical Biology Applications of Monocyclic Peptides

by

Siwen Wang

Doctor of Philosophy, Graduate Program in Environmental Toxicology
University of California, Riverside, September 2021
Dr. Min Xue, Chairperson

Peptides are one of the most promising platforms for drug development due to their biocompatibility, similarity, and diversity. Over the past few decades, it has been proven that peptides are practical tools in various therapeutic and diagnostic applications. Studies show that monocyclic peptides are capable of functioning as an effective alternative to complex molecules, such as antibodies or small molecules. In this dissertation, I describe projects that aimed at applying monocyclic peptides into the chemical biology field. The first chapter covers the screening procedures and results of a monocyclic peptide library in detail. Lipid A moiety was used as the screening target to demonstrate the therapeutic application of monocyclic peptides for LPS neutralization. Chapter 2 talks about the application of monocyclic peptides as imaging probes for protein activities in suspension cells. Digitonin, a cell membrane perforator will be introduced as the delivery mediator for the imaging probes. Analysis of AKT signaling activities on a single-cell level will be reported, including the demonstration of drug perturbation on the regulator proteins.

Chapter 3 will cover the application of monocyclic peptides as molecular transporters. A small library of monocyclic peptides capable of penetrating the cell membrane will be introduced in this project. These hydroxyl-rich cycle peptides will demonstrate the diversity of cargo molecules into more than ten different cell lines. The mechanisms and fate of these monocyclic peptides will be discussed, providing a thorough explanation of the cell-penetrating process. The discovery of this novel group of peptides with non-positive charges can bring more insights into the cell-penetrating peptide field.

Table of Contents

List of Figures

List of Tables

Chapter 1: Introduction

1.1 Current therapeutic molecules

Small chemical molecules (molecular weight <500 Da) are considered to date the most usable FDA-approved drugs capable of regulating a biological process. Nevertheless, one of the biggest limitations of small molecules is that they can only target proteins with well-defined binding pockets. Consequently, protein-protein interactions (PPIs) are usually not targetable by small molecules. To overcome such limitations, larger molecules (molecular weight >500 Da), such as antibodies, are developed as therapeutics since the 1980s. Although these macromolecules can reach challenging targets, but their applications are limited to extracellular targets because they are too large to enter the cells.[1] As an appropriate substitution for both molecules, peptides are considered the next-generation therapeutics due to their unique features. Peptides are biochemically and therapeutically distinct from small molecules and macromolecules, and their size is between them.[2] Peptides can be categorized into two broad structural classes: linear and cyclic peptides. Peptide macrocyclization can lead to conformational rigidity, higher target binding affinity and selectivity, improved metabolic stability and better membrane permeability, and, as such, is an important tool in peptide drug discovery. Particularly, monocyclic peptides provide more selective binding and uptake by the target receptor and higher potency and stability compared with their linear counterparts.[3]

1.2 The role of monocyclic peptides in therapeutics

Based on the discovered biological activities of naturally occurring monocyclic peptides, synthetic monocyclic peptides have constantly been studied and identified. Both types of

monocyclic peptides have been applied in diverse fields, including therapeutics, drug targeting, cell permeability improvement etc.

Enzyme inhibition

Several monocyclic peptides function as enzyme inhibitors among naturally occurring monocyclic peptides. One example is the peptidylprolyl isomerase Pin1, an enzyme targeting the Pro conformation in peptide sequences containing phosphorylated Thr/Ser where the Pro is located after them. Pin1 is famous for regulating the cell cycle by mediating cis-trans isomerization. Thus, it has been recognized as a target for cell cycle regulation. Pei and coworkers have developed a library composed of millions of different peptide compounds displaying on the microbead surface and developed an inhibitor with a nanomolar affinity towards the catalytic domain of Pin1.[4]

Cell Permeability improvement

It is easy to notice that cyclization can help improve membrane permeability. As mentioned above, cyclosporin A is cell-membrane permeable as a naturally occurring monocyclic peptide representative. Studies have shown that the intramolecular hydrogen bonds between the hydrophilic groups within cyclosporin A contribute to the membrane permeability. Other than naturally occurring monocyclic peptides, Lin and coworkers added a bisaryl cross-linker to a BH3 peptide-based Mcl-1 inhibitor, which has greatly improved the cellular uptake and inhibitory effect of the original peptide.[5] Importantly, this study pointed out that the hydrophobicity of the peptide structure is an essential factor in enhancing the cellular uptake of the peptides.

Receptor binding agents

Cell-surface receptors are usually good targets for monocyclic peptides because the peptides do not need to cross the cell membrane. For example, Park and coworkers have developed a mimetic sequence of a monoclonal antibody that can specifically recognize p185HER2/neu growth factor receptor.[6] The monocyclic peptide was cyclized by a disulfide linkage and can inhibit p185HER2/neu tyrosine kinases both *in vitro* and *in vivo.* Such monocyclic peptides can effectively bind to the receptor as an antagonist. A monocyclic tetrapeptide, CJ-15,208, is another example that is worth mentioning. It was isolated from a fungal fermentation broth with great affinity to the kappa opioid receptor. McLaughlin and coworkers have synthesized a tryptophan isomer of CJ-15,208 and demonstrated its specific antagonism for the receptor.[7, 8]

1.3 Motivation and contents of the studies in this thesis

Notable progress has been made in the research and therapeutic applications of monocyclic peptides, including imaging, diagnostics, enzyme inhibition, and receptor agonist/antagonist development. However, more studies are still needed to enhance the drug-like properties of monocyclic peptides, such as minimizing cytotoxicity, increasing target specificity, improving cell-penetrating ability and oral absorption etc. In our work, we have looked into the following areas including finding binders for complex molecules through monocyclic peptide library screening, interrogating protein signaling activities using monocyclic probes inside the cells enabled by a generalized cell permeabilizer, as well as the design and study of using monocyclic peptides as promising cargo delivery tools.

In chapter 2, we will talk about the combinatorial screening of monocyclic peptides against Lipid A. LPS was known to induce an innate immune response, which can cause the overexpression of cytokines, leading to inflammatory diseases such as sepsis. As mentioned before, LPS cannot be targeted by small molecules due to the lack of a well-defined structure. Besides, all the monoclonal antibodies been discovered have failed clinical studies because they can only recognize lipid A in its non-native form.[9] One of the monocyclic peptide drugs targeting LPS involves the toxicity concern since it lacks specificity.[10] Therefore, our first study will demonstrate the feasibility of identifying a non-toxic monocyclic peptide binder for LPS-bound lipid A through a combinatorial library screening.

In chapter 3, we will introduce the digitonin-facilitated delivery of monocyclic peptides enabling single-cell analysis of AKT signaling activities in suspension cells. AKT protein, also known as protein kinase B, it helps regulate cell metabolism, cell growth, proliferation, and survival. It also plays a crucial role in the transcription and protein synthesis process. The hyperactivation of AKT protein could lead to lots of diseases such as cancer, diabetes, cardiovascular and neurological diseases etc.[11] In this project, we used a pair of monocyclic peptides that bind with AKT at different regions to interrogate its signaling dynamics. Liposomes were used to deliver the peptide probes inside a glioblastoma cell line in our previous studies.[12] However, the delivery method can not be universally applied to suspension cell lines such as actual patient biopsy samples. So we improved the delivery method to enable the investigation of the connection between kinetic patterns of AKT signaling and the AKT expression levels in both lymphoid and myeloid suspension cells.

Lastly, in chapter 4, we will look into the hydroxyl-rich endocytosis-promoting monocyclic peptides. Cell-penetrating peptides have been a popular field for several decades.[13-16] Nevertheless, the enhancement of delivering efficacy of cell-penetrating peptides still calls for future study. Other than that, the mechanisms of lots of penetration processes for monocyclic peptides still remain unknown. Our final study focused on the design of a group of untraditional cell-penetrating peptides. We also investigated their penetrating mechanism and showcased a novel receptor-mediated endocytosis pathway out peptide was taken.

Overall, our studies have identified monocyclic peptide binders for not-well-defined targets, successfully delivered monocyclic peptide probes inside suspension cells for protein investigation, and helped expand the cell-penetrating peptide pool as as well as enriching the mechanisms for cell membrane penetration.

1.4 References

1. Rhodes, C. A.; Pei, D., Bicyclic peptides as next-generation therapeutics. *Chemistry (Weinheim an der Bergstrasse, Germany)* **2017,** *23* (52), 12690.

2. Lau, J. L.; Dunn, M. K., Therapeutic peptides: Historical perspectives, current development trends, and future directions. *Bioorganic & medicinal chemistry* **2018,** *26* (10), 2700-2707.

3. Edman, P., Chemistry of amino acids and peptides. *Annual review of biochemistry* **1959,** *28* (1), 69-96.

4. Liu, T.; Liu, Y.; Kao, H.-Y.; Pei, D., Membrane permeable cyclic peptidyl inhibitors against human Peptidylprolyl Isomerase Pin1. *Journal of medicinal chemistry* **2010,** *53* (6), 2494-2501.

5. Muppidi, A.; Doi, K.; Ramil, C. P.; Wang, H.-G.; Lin, Q., Synthesis of cell-permeable stapled BH3 peptide-based Mcl-1 inhibitors containing simple aryl and vinylaryl cross-linkers. *Tetrahedron* **2014,** *70* (42), 7740-7745.

6. Park, B.-W.; Zhang, H.-T.; Wu, C.; Berezov, A.; Zhang, X.; Dua, R.; Wang, Q.; Kao, G.; O'Rourke, D. M.; Greene, M. I., Rationally designed anti-HER2/neu peptide mimetic disables p185 HER2/neu tyrosine kinases in vitro and in vivo. *Nature biotechnology* **2000,** *18* (2), 194-198.

7. Ross, N. C.; Kulkarni, S. S.; McLaughlin, J. P.; Aldrich, J. V., Synthesis of CJ-15,208, a novel κ-opioid receptor antagonist. *Tetrahedron letters* **2010,** *51* (38), 5020-5023.

8. Ross, N. C.; Reilley, K. J.; Murray, T. F.; Aldrich, J. V.; McLaughlin, J. P., Novel opioid cyclic tetrapeptides: Trp isomers of CJ-15,208 exhibit distinct opioid receptor agonism and short-acting κ opioid receptor antagonism. *British journal of pharmacology* **2012,** *165* (4b), 1097-1108.

9. Matyas, G. R.; Beck, Z.; Karasavvas, N.; Alving, C. R., Lipid binding properties of 4E10, 2F5, and WR304 monoclonal antibodies that neutralize HIV-1. *Biochimica et Biophysica Acta (BBA)-Biomembranes* **2009,** *1788* (3), 660-665.

10. Tsuzuki, H.; Tani, T.; Ueyama, H.; Kodama, M., Lipopolysaccharide: neutralization by polymyxin B shuts down the signaling pathway of nuclear factor κB in peripheral blood mononuclear cells, even during activation. *Journal of Surgical Research* **2001,** *100* (1), 127-134.

11. Fayard, E.; Tintignac, L. A.; Baudry, A.; Hemmings, B. A., Protein kinase B/Akt at a glance. *Journal of cell science* **2005,** *118* (24), 5675-5678.

12. Shao, S.; Li, Z.; Cheng, H.; Wang, S.; Perkins, N. G.; Sarkar, P.; Wei, W.; Xue, M., A Chemical Approach for Profiling Intracellular AKT Signaling Dynamics from Single Cells. *Journal of the American Chemical Society* **2018,** *140* (42), 13586-13589.

13. Zou, L.; Peng, Q.; Wang, P.; Zhou, B., Progress in research and application of HIV-1 TAT-derived cell-penetrating peptide. *Journal of Membrane Biology* **2017,** *250* (2), 115.

14. Thorén, P. E.; Persson, D.; Karlsson, M.; Nordén, B., The antennapedia peptide penetratin translocates across lipid bilayers–the first direct observation. *FEBS letters* **2000,** *482* (3), 265-268.

15. Edwards, A. B.; Anderton, R. S.; Knuckey, N. W.; Meloni, B. P., Characterisation of neuroprotective efficacy of modified poly-arginine-9 (R9) peptides using a neuronal glutamic acid excitotoxicity model. *Molecular and cellular biochemistry* **2017,** *426* (1-2), 75-85.

16. Qian, Z.; Martyna, A.; Hard, R. L.; Wang, J.; Appiah-Kubi, G.; Coss, C.; Phelps, M. A.; Rossman, J. S.; Pei, D., Discovery and mechanism of highly efficient cyclic cell-penetrating peptides. *Biochemistry* **2016,** *55* (18), 2601-2612.

Chapter 2: Combinatorial screening of monocyclic peptides against lipid A

2.1 Introduction

Gram-negative bacterial infection accounts for more than half a million severe sepsis cases annually in the US,[1-4] where lipopolysaccharide (LPS) and its toxic component, lipid A,[3-6] are major pathogenic factors. With the assistance of LPS-specific proteins, high levels of LPS continuously hyper-activates the toll-like receptor (TLR4) signaling cascade and unleashes a dangerous amount of pro-inflammatory cytokines (Fig. 2.1). [3] This process is accompanied by a compensatory release of anti-inflammatory cytokines, which suppresses the immune system and interferes with pathogen clearance.[3, 7-8] The cumulated effects cause severe sepsis and septic shock.

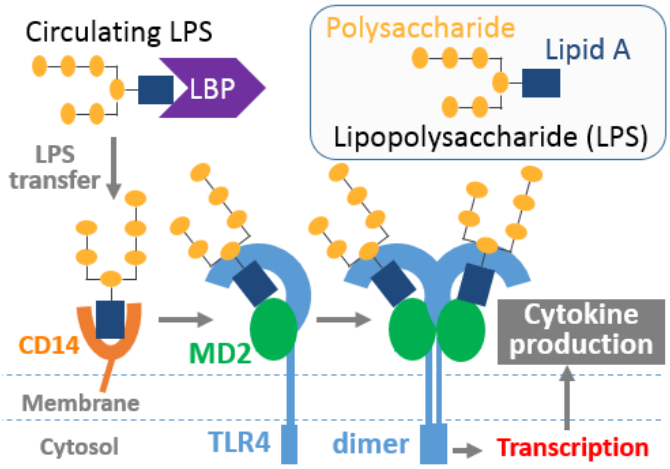

Fig. 2.1 LPS activates the TLR4 pathway. The lipid A moiety is crucial for the recognition and transportation of LPS.

Effective therapeutic managements for gram-negative infection-caused sepsis remain challenging, despite that the molecular mechanism of disease progression is clear.[9] Therapies that block TLR4 activation and neutralize the effector cytokines failed to demonstrate efficacy in clinical trials.[7-9] Because high levels of LPS initiates and continuously fuels the signaling events, it was reasoned that lowering the LPS level would

be beneficial to septic patients. This hypothesis led to the development of monoclonal antibodies (mAbs) against LPS. However, those mAbs failed in clinical trials.[9-12] Retro-analysis revealed that mAbs could not recognize the lipid A moiety effectively and therefore did not fully engage the target.[7, 13-14]

Derivations based on LPS-binding proteins have led to various LPS-neutralizing peptides. For example, peptide fragments from the human LBP can inhibit the binding of circulating LPS to LBP and block LPS-induced tumor necrosis factor (TNF-α) release *in vitro* and *in vivo*.[15] A synthetic peptide derived from the cationic antimicrobial protein (azurocidin) attenuates the toxic effects of *Escherichia coli* LPS *in vivo* in a dose-dependent manner.[16] LPS-binding components with non-human origins have also been studied. For instance, a cyclic peptide based on the *Limulus* anti-LPS factor can effectively block LPS-induced TNF-α production in mice models.[17]

In addition to protein-derived structures, naturally occurring antimicrobial peptides, such as polymyxin B (Fig. 2.2), are among the most potent LPS-neutralization agents. For instance, hemoperfusion using immobilized polymyxin B could effectively remove circulating LPS and has demonstrated to be beneficial to septic patients.[18] However, because of their nonselective binding to cell membranes, these peptides exhibit prominent neurotoxicity and nephrotoxicity. Consequently, their applications are limited.

Clinical evidence proves that LPS-neutralization is a viable therapeutic option for the management of septic patients, but LPS-binding agents suitable for intravenous injection remain underdeveloped. There are limited varieties of naturally occurring LPS-binding molecules, and in many cases, their LPS-neutralization potency accompanies toxicity. On

the other hand, several major obstacles exist in adapting *de novo* drug discovery approaches (ie. high throughput screening) to develop new LPS-neutralizing structures. Those challenges include the absence of binding pockets, the highly heterogeneous components of LPS, and the lack of effective strategies for targeting the lipid A moiety, which is crucial for neutralization.

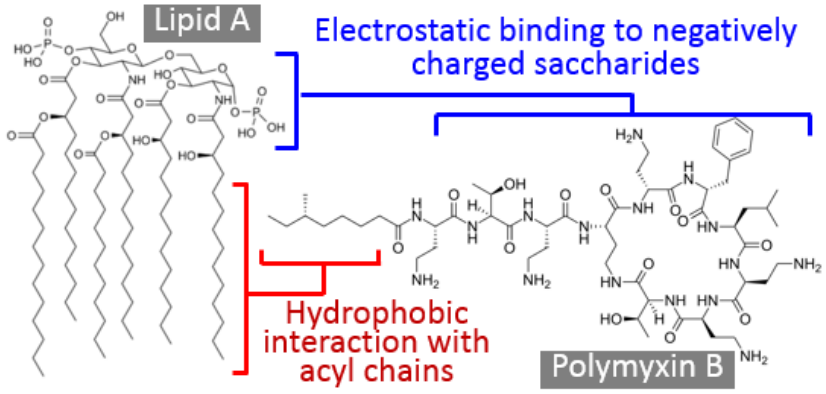

Fig. 2.2 Polymyxin B binds to lipid A through nonspecific interactions. PB interacts with any membrane and therefore is highly toxic. Lipid A structures have large varieties, which is not shown here.

Herein, we hypothesize that we can discover new LPS-neutralizing compounds by using ultrahigh capacity cyclic peptide libraries and lipid-A targeting modular screening approaches. Our hypothesis is based on recent developments in our group. [19-20] First, we have unique one-bead-one-compound (OBOC) cyclic and bicyclic peptide libraries exhibiting a diverse and well-defined chemical space. Second, we established automated protocols for screening ultrahigh capacity libraries. Third, we streamlined robust chemical methods for de novo sequencing of library components. Finally, we synthesized a Rhodamine-phenylboronic acid fluorescent dye for nonselective labeling of the polysaccharides on LPS, enabling negative panning against lipid A moieties.

The success of the project promises novel LPS-neutralizing structures as the basis for further medicinal optimization. It also helps understand the structure-function relationship in LPS toxicity and sepsis pathogenesis.

2.2 Experimental

Chemicals and reagents

TentaGel S-NH2 resin (loading capacity 0.28 mmol/g) was purchased from Rapp Polymere GmbH and Rink amide MBHA resin (loading capacity 0.678 mmol/g) from Aapptec (Louisville, KY). All the Fmoc-protected amino acids were purchased from Anaspec (Fremont, CA) except Fmoc-L-propargylglycine (Pra) and FmocLys(N3)-OH (Az4), which were purchased from Chempep (Wellington, FL) and Chem-Impex (Wood Dale, IL), respectively. The coupling reagent 2-(1H-benzotriazol-1-yl)-1,1,3,3-tetramethyluronium hexafluorophosphate (HBTU, 99.6%) was obtained from Chem-Impex (Wood Dale, IL). Diisopropylethylamine (DIEA, 99.5%) was purchased from ACROS (Germany). Phenyl isothiocyanate (PhNCS) and triisopropylsilane (TIPS) were obtained from TCI (Portland, OR). Piperidine was purchased from Alfa Aesar (Ward Hill, MA). Cyanogen bromide (CNBr) was obtained from ACROS (Pittsburg, PA). Rhodamine B (Rhod), cuprous iodide (CuI), α-cyano-4-hydroxycinnamic acid (CHCA), Lipopolysaccharides from different bacteria strains (LPS), Phenylboronic acid (PBA) and Polymyxin B solution (1 mg/mL in H_2O) were obtained from Sigma-Aldrich (St. Louis, MO). Tris base, sodium phosphate dibasic anhydrous (Na2HPO4, 99.6%), sodium phosphate monobasic monohydrate (NaH2PO4, 99.4%), sodium chloride (NaCl), ascorbic acid, Tween 20, sodium dodecyl sulfate (SDS), bovine serum albumin (BSA), acetonitrile (CH3CN), diethyl ether (Et2O),

chloroform (CHCl3), ethyl acetate (EA), N,N′-dimethylformamide (DMF), and dichloromethane (DCM) were purchased from Thermo Fisher Scientific (Waltham, MA).

Preparative Reversed-Phase (RP) High-Performance Liquid Chromatography (HPLC)

Preparative HPLC was performed on a Thermo Ultimate 3000BX HPLC instrument, using a Phenomenex C18 reversed-phase preparative column (Kinetex 5 μm EVO, 250 × 21.2 mm^2). Nonlinear gradients of 0−100% acetonitrile (with 0.1% TFA) in water (with 0.1% TFA) were employed, and the gradient parameters were adjusted for each product to achieve desired separation efficiencies. A multiwavelength UV−vis detector was used to monitor the absorbance at 215, 280, 480, and 560 nm.

Analytical HPLC.

The purity of the peptide was analyzed on a Thermo Ultimate 3000SD HPLC instrument, using a Phenomenex C18 reversed-phase analytical column (Kinetex 2.6 μm EVO, 250 × 4.6 mm^2). A gradient of 0−100% acetonitrile (with 0.1% TFA) in water (with 0.1% TFA) was employed with a flow rate of 1.5 mL/min. A UV−vis detector was used to monitor the absorbance at 280 or 560 nm. The purity of all cyclic peptides used for binding assays and biological activity assays was >95%.

Mass Spectrometry

The MS and MS/MS spectra were obtained using a SCIEX 5800 matrix-assisted laser desorption ionization time-of-flight (MALDI-TOF) mass spectrometer.

Solid-Phase Peptide Synthesis

The peptides were synthesized following the standard Fmoc SPPS coupling process. Unless otherwise noted, Rink Amide MBHA resin was used for the synthesis. To couple

amino acids to the resin, the Fmoc group on the resin was first removed by 20% piperidine/DMF solution (10 min, three times). Fmoc-AA-OH (3 equiv), DIEA (5 equiv), and HBTU (2.8 equiv) were mixed in DMF for 10 min, and the solution was then introduced to the deprotected resin. The mixture was gently rotated at room temperature for 1 h, followed by draining and washing with DMF for three times. To label the peptides with fluorophores, the corresponding dye-COOH was coupled at the N-terminal using the SPPS procedure described above.

For constructing cyclic peptides, Fmoc-propargylglycine-OH (Pra) and Fmoc-azidolysine-OH (Az4) were inserted at the N and C terminals, respectively. A Cu-catalyzed click reaction was used for cyclization. Specifically, resins were incubated in 20% lutidine/ DMF with CuI (2.5 equiv) and L-ascorbic acid (5 equiv) at room temperature rotating overnight. After cyclization, the beads were washed with sodium diethyldithiocarbamate (5% w/v) and DIEA (5% v/v) in DMF to remove the copper catalyst. After that, the beads were rinsed with DMF five times to get rid of the wash solution for click reaction. To cleave peptides off the resin, a cleavage solution composed of TFA/TIPS/ddH2O (95:2.5:2.5) was used. Then the peptides were purified by preparative RP-HPLC, and the product purity and identity were confirmed by analytical RP-HPLC and mass spectrometry.

Rhodamine-phenylboronic acid (RhPBA) synthesis

For the synthesis of RhPBA, 1.86 mmol of phenylboronic acid, 1.86 mmol of 1-ethyl-3-(3-dimethylaminopropyl)-carbodiimide (EDC), 1.86 mmol of 1-hydroxybenzotriazole (HOBt), 1.86 mmol of Rhodamine B and 3.72 mmol of 4-dimethylaminopyridine (DMAP) was added to 30 ml of dichloromethane (DCM). The mixture was stirred overnight, covered

with aluminum foil. The solution was diluted in DCM the next day before being extracted with H_2O three times. The organic phase was collected and continue to be extracted with Brine once to remove extra water in the system. After that, sodium sulfate anhydrous was added to the solution to further dry the solution. The product was filtered and evaporated to reach a solid state and was purified by preparative RP-HPLC, and the product purity and identity were confirmed by analytical RP-HPLC and mass spectrometry.

One-Bead−Two-Compound (OBTC) Library Construction

The one-bead−two-compound peptide library was constructed using the split-and-pool strategy on TentaGel S-NH2 resins. Methionine was first coupled to the resin, followed by glycine. Then, Az4 was coupled at 80% loading capacity. Eighteen natural amino acids (Ala, Arg, Asn, Asp, Gln, Glu, Gly, His, Ile, Leu, Lys, Phe, Pro, Ser, Thr, Trp, Tyr, and Val, all L-stereoisomers) were used as building blocks for the subsequent five randomized positions, and a Pra residue was attached at the N-terminal. The library was cyclized, as described above. Afterward, an additional Pra was attached to the N-terminal. The protecting groups were removed as described above. The deprotected resins were then washed with DMF, methanol, and DCM and kept under Argon for further use.

OBTC Library Screening.

Three types of LPS molecules will be employed as screening targets: LPS from (Table 1). These bacteria represent the leading causes of gram-negative sepsis.[1, 2] They also represent different types of LPS and lipid A structures.[3-5] We choose one representative type for each bacteria in our screening. The corresponding LPS and Lipid A from these strain types are

commercially available with ultrahigh purity, which will facilitate our screening and validation processes. In addition, their LPS structures have been elucidated.

Bacteria	* Strain Type
Escherichia coli	O55:B5
Klebsiella pneumoniae	NCTC418
Pseudomonas aeruginosa	PD-05140

Table 2.1 Selected LPS targets. *Chosen based on the commercial availability of corresponding ultrapure LPS.

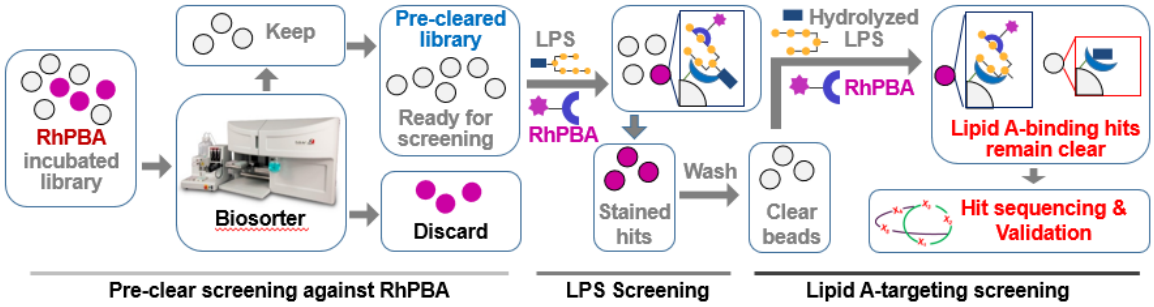

Fig. 2.3 The proposed modular screening strategy. RhPBA is used to recognize the polysaccharide part of LPS, which enables the identification of polysaccharide-binding versus lipid A-binding beads.

Sequencing of the Hits: Edman Degradation

The first round of Edman degradation was performed to remove the click handle that was conjugated to the epitope.[6] The hit beads were transferred into a glass vial with 50 μL of 2.5% PhNCS in pyridine/H_2O (1:1) solution and flushed with Ar for about 15 s. The vial was then placed in a water bath at 50 °C for 30 min, and the solution was removed. The beads were then washed with ethyl acetate (three times) and DCM (once) and air-dried. Subsequently, 100 μL of TFA solution was added to the vial, flushed with Ar, and left for incubation in the water bath for 10 min at 50 °C. Afterward, the solution was removed, and

the beads were washed three times with ethyl acetate and then with DCM. These procedures were repeated for another round of Edman degradation. Later the beads were incubated with a 20% TFA/water solution and heated at 60 °C for 15 min. After 15 min, the solution was removed, and the beads were washed with ethyl acetate and DCM and then air-dried.

Cleavage

After the Edman degradation, individual beads were transferred into a microcentrifuge tube containing 10 μL of water and 10 μL of a 0.5 M CNBr/0.2 M HCI solution. The tubes were microwaved for 1 min and dried using a centrifugal vacuum chamber at 45 °C.[7]

Sequencing by MALDI-TOF MS/MS

First, 0.55 μL of a 4 mg/mL α-cyano-4-hydroxycinnamic acid (CHCA) solution (50:50 ACN/water with 0.1% TFA) was added in each microcentrifuge tube. The mixture was spotted on a 384-spot MALDI sample plate and air-dried. The MS/MS spectra were obtained on a SCIEX 5800 mass spectrometer and analyzed using mMass to solve for the sequences.[8]

Enzyme-linked immunosorbent assay (ELISA)

THP-1 cells are seeded at 10K with different peptide ligands at 10 mg/ml in a 96-well plate. LPS solution was diluted with media and added to each sample. The supernatant from each well was collected after 4 hours. The harvest solutions were centrifuged to get rid of cells. The amount of cytokines (TNF-alpha) released by the cells under different treatment was measured using a Human TNF-alpha Duoset ELISA kit purchased from R&D systems.

Resazurin assay

The resazurin is a redox dye used as an indicator for an active metabolism in cell culture. It is based on the reduction of resazurin to resorufin by using NADH or NADPH as electron donors in metabolically active cells. THP-1 cells treated with different concentrations of ligands were seeded in a 96-well plate and incubated for 4 hours. 40 μL of 0.06 mg mL−1 resazurin solution (in cell culture media) was then added into each well, followed by incubation at 37 °C for 3 hours. The resulted fluorescence signals were recorded by a plate reader (560 nm excitation, 590 nm emission).

2.3 Results and Discussion

Ultra-high throughput screening generated hit sequences

Previous development of LPS-binding peptides depends on iterations of known antimicrobial peptides or LPS-binding proteins, leading to limited structural varieties. We propose to perform automated large-scale library screening where around 4 million cyclic peptide structures are screened for LPS binding hits. This covers a large chemical space and provides new lead structures.

We chose a monocyclic peptide structure with functional and spatial diversities (Fig. 2.4).[9-11] These peptides have rigid backbones that enable high-affinity binding due to "pre-paid entropy" effects. In contrast to polymyxin B, these cyclic peptides lack hydrophobic tails, therefore, are expected to be of low cytotoxicity.

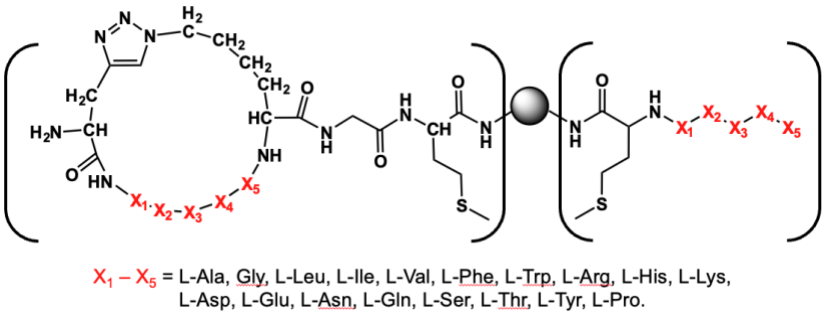

Fig. 2.4 The structures of the monocyclic peptide library.

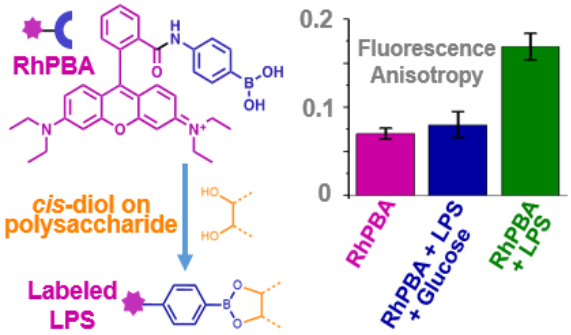

Fig. 2.5 (Left) Rhodamine-phenylboronic acid binds with *cis*-diol on polysaccharides, forming boronic esters. It labels both intact and hydrolyzed LPS. (Right) Fluorescence anisotropy results prove the binding of RhPBA to LPS. Glucose can displace LPS and bind to RhPBA, causing a decreased anisotropy.

We have synthesized and characterized the saccharide-reactive dye (RhPBA), and validated its reactivity towards the polysaccharide part in LPS (Fig. 2.5). The binding between LPS and RhPBA was confirmed using fluorescence polarization tests. Because LPS molecules often form large aggregates in the solution, the RhPBA bound to LPS have higher fluorescence anisotropy in the solution, comparing to that of free RhPBA (Fig. 2.5). RhPBA binds to *cis*-diols with minimal selectivity; therefore, adding excess glucose into the system will disrupt the RhPBA/LPS binding and decrease the fluorescence anisotropy (Fig. 2.5). When screening against hydrolyzed LPS (polysaccharide and lipid A mixture),

this labeling allows clear identification of lipid A-specific hits from polysaccharide-specific hits. This result proved the covalent binding nature between RhPBA and LPS, pointing to the feasibility of the proposed modular screening strategy.

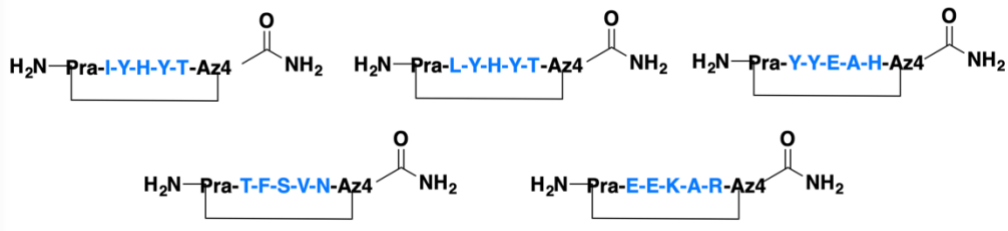

Fig. 2.6 Identified hits from the pilot screening.

As described in Fig. 2.3, RhPBA allows us to perform the modular screening process. To test the feasibility of the proposed modular screening strategy, we conducted a pilot screening using 100 k beads from the monocyclic library against ultrapure LPS from *Escherichia coli* (O55:B5). We obtained five hit beads, all of which were successfully sequenced using mass spectrometry (Fig. 2.6). Compared to the highly positively charged polymyxin B, these hits did not bear high positive charges, pointing to a new lipid A-recognition mechanism. This absence of positive charge may contribute to less toxicity in LPS-neutralization applications.

Assess the LPS neutralization effect on myeloid cells (THP-1 cells)

THP-1 cells are of the myeloid lineage and are widely used in immunology studies. They are known to produce cytokines in response to LPS-stimulation. We synthesized both linear and cyclic versions for all the hit peptides. We challenged those cells with LPS in the presence of the peptides and quantified the resulted cytokine production levels (Fig. 2.7). The results showed that one of the hit peptides, cy(LYHYT), exhibited LPS neutralization

effects which lead to a minor degree of decreased cytokine production (Fig. 2.8). Our result demonstrated the feasibility of identifying monocyclic peptide ligands for a complex target via the combinatorial screening of a monocyclic library. In addition, we also performed a resazurin assay on THP-1 cells incubated with two representative monocyclic hit sequences in a concentration gradient manner. The result indicated that the signal intensity of the treated cells is pretty much the same level as for the control group (no treatment), which further confirmed our hypothesis that without positive charges, our monocyclic peptide would exhibit a low cytotoxicity on THP-1 cells in terms of LPS neutralization (Fig. 2.9).

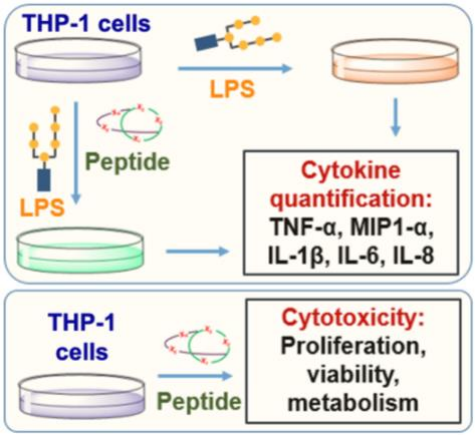

Fig. 2.7 (Upper) Quantification of cytokine production for the evaluation of LPS-neutralizing abilities of peptides. (Lower) Testing the toxicity of the identified peptides.

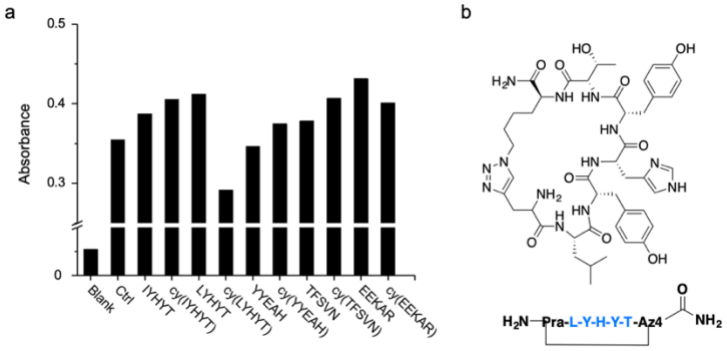

Fig. 2.8 (**a**) LPS neutralization effect of both linear and cyclic versions of the hit peptides. (**b**) A representative structure for the hit peptides.

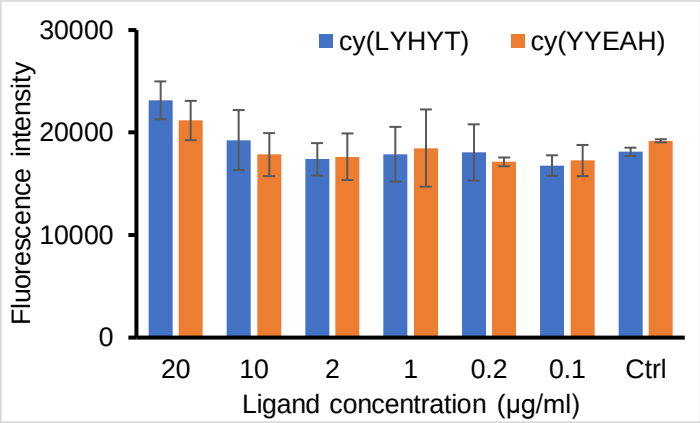

Fig. 2.9 Resazurin assay result for the evaluation of the cytotoxicity of representative ligands, cy(LYHYT) and cy(YYEAH).

2.4 Conclusion

In conclusion, we have synthesized and screened a combinatorial monocyclic peptide library against the toxic moiety of LPS. The modular screening process contains three steps. First, we labeled the library with RhPBA and used the Biosorter instrument to exclude beads with nonspecific binding, which is crucial for the validity of subsequent steps. Second, the pre-cleared library was incubated with a mixture of LPS and RhPBA in order to screen out library components with high affinities to LPS absorbed LPS on the surface. Third, the LPS-specific beads were incubated with RhPBA and hydrolyzed LPS (a mixture of lipid A and polysaccharide) after removing the bound LPS/RhPBA by thorough washing. Consequently, beads that bind with polysaccharides were stained by RhPBA, and by contrast, the lipid A-specific ones remained clear due to the lack of surface polysaccharides. Using the hits from the screening, we further measured the LPS neutralization ability of each hit monocyclic peptide by quantifying the cytokine release of peptide/LPS-treated THP-1 cells. Our results showcased the feasibility of identifying hit sequences against a

complex target like LPS, underscored the possibility of a novel LPS-neutralization compound with much lower toxicity comparing to the current solutions.

Since the LPS inhibitory effect of our peptides appeared to be limited, more screening efforts using other libraries should be explored in future research. For example, more complex libraries composed of bicyclic peptides can be employed for screening, which might promise higher binding affinities due to the rigid backbones.

2.5 References

1. Angus, D. C.; Van der Poll, T., Severe sepsis and septic shock. *N Engl J Med* **2013,** *369*, 840-851.

2. Opal, S. M.; Garber, G. E.; LaRosa, S. P.; Maki, D. G.; Freebairn, R. C.; Kinasewitz, G. T.; Dhainaut, J.-F.; Yan, S. B.; Williams, M. D.; Graham, D. E., Systemic host responses in severe sepsis analyzed by causative microorganism and treatment effects of drotrecogin alfa (activated). *Clinical infectious diseases* **2003,** *37* (1), 50-58.

3. Kato, N.; Sugiyama, T.; Naito, S.; Arakawa, Y.; Ito, H.; Kido, N.; Ohta, M.; Sasaki, K., Molecular structure of bacterial endotoxin (Escherichia coli Re lipopolysaccharide): implications for formation of a novel heterogeneous lattice structure. *Molecular microbiology* **2000,** *36* (4), 796-805.

4. Vinogradov, E.; Frirdich, E.; MacLean, L. L.; Perry, M. B.; Petersen, B. O.; Duus, J. Ø.; Whitfield, C., Structures of lipopolysaccharides from Klebsiella pneumoniae: Elucidation of the structure of the linkage region between core and polysaccharide O chain and identification of the residues at the non-reducing termini of the Ochains. *Journal of Biological Chemistry* **2002,** *277* (28), 25070-25081.

5. Pier, G. B., Pseudomonas aeruginosa lipopolysaccharide: a major virulence factor, initiator of inflammation and target for effective immunity. *International journal of medical microbiology* **2007,** *297* (5), 277-295.

6. Klemm, P., Manual Edman degradation of proteins and peptides. In *Proteins*, Springer: 1984; pp 243-254.

7. Lee, S. S.; Lim, J.; Cha, J.; Tan, S.; Heath, J. R., Rapid microwave-assisted CNBr cleavage of bead-bound peptides. *Journal of combinatorial chemistry* **2008,** *10* (6), 807.

8. Niedermeyer, T. H.; Strohalm, M., mMass as a software tool for the annotation of cyclic peptide tandem mass spectra. **2012**.

9. Li, Z.; Shao, S.; Ren, X.; Sun, J.; Guo, Z.; Wang, S.; Song, M. M.; Chang, C.-e. A.; Xue, M., Construction of a sequenceable protein mimetic peptide library with a true 3D diversifiable chemical space. *Journal of the American Chemical Society* **2018,** *140* (44), 14552-14556.

10. Shao, S.; Li, Z.; Cheng, H.; Wang, S.; Perkins, N. G.; Sarkar, P.; Wei, W.; Xue, M., A Chemical Approach for Profiling Intracellular AKT Signaling Dynamics from Single Cells. *Journal of the American Chemical Society* **2018,** *140* (42), 13586-13589.

11. Das, S.; Nag, A.; Liang, J.; Bunck, D. N.; Umeda, A.; Farrow, B.; Coppock, M. B.; Sarkes, D. A.; Finch, A. S.; Agnew, H. D., A general synthetic approach for designing

epitope targeted macrocyclic peptide ligands. *Angewandte Chemie International Edition* **2015,** *54* (45), 13219-13224.

Chapter 3: Digitonin-facilitated delivery of monocyclic peptides enables single-cell analysis of AKT signaling activities in suspension cells

3.1 Introduction

Signaling proteins are critical governors of cellular activities. In many biological systems, the expression levels of signaling proteins are highly heterogeneous among the same group of cells.[1,2] Understanding this heterogeneity through single-cell protein assays can help identify unique subpopulations and guide therapeutic decisions.[3,4] For instance, cells with higher oncoprotein levels often represent a drug-resistant phenotype, and targeting these cells using combination chemotherapies can provide long-lasting effects.[5–8] However, despite the rapid development in the field of single-cell protein analysis, little is known about the heterogeneity in the time domain, i.e., the dynamical features of protein signaling. Increasing evidence has demonstrated that the distinct temporal patterns of kinase signaling, such as oscillations, carry information that controls the cell's specific response and dictates cell fates.[9–11] Scrutinizing these dynamical behaviors of kinase signaling can help understand how various regulatory circuits shape signaling outputs.[11] Such a task is challenging since traditional immunolabeling-based analytical methods cannot be used inside living cells. Pioneering work on generic- ally encoded reporting systems has enabled real-time readouts of kinase signaling activities.[12–16] However, there remain two critical challenges. First, these reporters focus on specific substrate sequences and subcellular locations. This design is perfect for delineating the signaling architecture but not well-suited for assessing the global status of signaling protein activities. Second, the expression

of these reporters cannot be easily performed in delicate samples such as patient biopsies, which limits their translational applications.

To address these unmet needs, we have recently developed a chemical method to analyze single-cell kinase signaling dynamics, using cyclic peptide-based imaging probes that target specific kinase epitopes (Fig. 3.1a).[17] Compared with genetic approaches,[12,13,18,19] our chemical probes provide a more direct readout of the signaling activities, which is not limited by a particular substrate type or influenced by the distribution of the kinase targets. In addition, these probes can be easily removed upon cell fixation, thereby permitting down- stream single-cell analysis such as immunofluorescence-based protein quantification and enabling phenotype identifications.[17] Nevertheless, our original method required fusogenic liposomes to carry fluorescent probes into living cells, which can only be implemented in adherent cells. This requirement significantly limits the translational value of our original approach because of two reasons. First, blood samples are the most widely used and accessible clinical samples, which contain a rich repertoire of lymphoid and myeloid suspension cells.[20–22] Second, transforming clinical tumor samples into single-cell suspensions is straightforward and quick, but re-establishing them as adherent cells is a time-consuming and challenging process. Therefore, we need to improve our method, especially the probe delivery approach, to enable the analyzes of suspension cells.

A popular technique for bringing small molecules into the intracellular space is to append a cell-penetrating tag.[23,24] These tags include hydrophobic moieties that enable direct membrane penetration, as well as endocytosis-promoting groups such as poly-cationic residues and receptor substrate sequences such as RGD. Many examples have

demonstrated the successful applications of these cell-penetrating tags; however, all those tags require chemical modifications to the molecular probes. Such a requirement could be detrimental to our intended applications, as our cyclic peptide probes are sensitive to modifications – complete loss of binding often occurs after simple structure alterations. In addition, the cytosolic delivery efficiency of these tags often varies significantly across different payloads. Considering that our cyclic peptide probes have different structures, we reasoned that cell-penetrating tags may not be an easily generalizable approach.

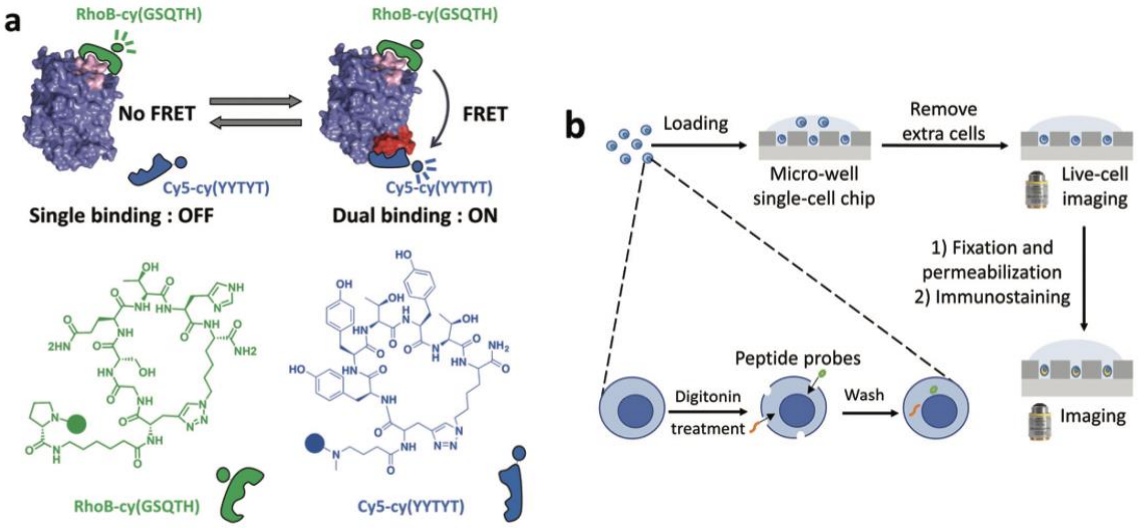

Fig. 3.1 (**a**) The mechanism of interrogating AKT signaling activities using a pair of cyclic peptide probes. (**b**) Digitonin can transiently permeabilize the cells and allow the peptide probes to diffuse into the cells. The cells can then be loaded onto a single-cell microwell chip for AKT signaling analysis.

Another method for cytosolic delivery involves membrane perforation. Physical perforation strategies, such as magnetoporation,[25] sonoporation[26] and optoporation,[27] can enable the transportation of large molecules and have demonstrated their applications in gene delivery. However, those manipulations are time-consuming, and they all require

specialized instruments, which also limits their generalizability and suitability in our analytical scheme. On the other hand, chemical perforators such as saponins are known to induce transient pores on the cell membrane, where the degree of perforation is often tunable by varying the saponin concentration.[28,29] These pores allow extracellular probe molecules to diffuse into the cytosol without any modifications to the probes. Encouraged by pioneering works on saponin-enabled peptide delivery,[30–32] we hypothesized that we could also use saponins to deliver the cyclic peptide probes into suspension cells.

Herein, we show that digitonin – a type of saponin – can indeed allow peptide probes to enter the cytosol of suspension cells (Fig. 3.1b). Using the cyclic peptide probes specific for detecting AKT activities, we demonstrate that this approach is applicable to different suspension cells, including adherent cells that are made into a single-cell suspension, myeloid cells, and lymphoid cells. We further show that this delivery approach is compatible with downstream immunofluorescence-based protein analysis by delineating the relationship between AKT expression level and the kinetic features of AKT signaling activities in THP-1 and Jurkat cells.

3.2 Experimental

Chemicals and reagents

Mannitol, HEPES, potassium chloride (KCl), sodium succinate, ethylene glycol-bis(β-aminoethyl ether)-N,N,N′,N′-tetra- acetic acid (EGTA), ethylenediaminetetraacetic acid (EDTA), bovine serum albumin (BSA), resazurin, (3-(4,5-dimethyl- thiazol-2-yl)-2,5-diphenyltetrazolium bromide (MTT), and digitonin were purchased from Sigma-Aldrich (St Louis, MO). Phosphate-buffered saline (PBS), Dulbecco's modified Eagle's medium

(DMEM), RPMI media, penicillin–streptomycin (pen– strep), and heat-inactivated fetal bovine serum (FBS) were purchased from Thermo Fisher Scientific (Waltham, MA).

Cell culture

All cells were purchased from ATCC (the American Type Culture Collection). U87 cells were cultured in DMEM with 10% FBS and 100 U mL^{-1} of pen–strep. THP-1 cells and Jurkat cells were cultured in RPMI-1640 with 10% FBS and 100 U mL^{-1} of pen–strep. All cell cultures were maintained in a humidified 5% CO_2 (v/v) incubator at 37 °C.

Digitonin treatment

Cells were washed three times in mannitol experiment buffer (MEB) before digitonin treatment. The washed cells were resus- pended in MEB buffer and incubated with digitonin (various concentrations) for 20 minutes, with or without the presence of the peptide probes. Afterwards, the cells were washed three times with fresh culture media to ensure the removal of digitonin.

Cell viability tests

Resazurin assay. Cells treated with different concentrations of digitonin were seeded in a 96-well plate and incubated for 5 hours. 40 μL of 0.06 mg mL^{-1} resazurin solution (in cell culture media) was then added into each well, followed by incubation at 37 °C for 3 hours. The resulted fluorescence signals were recorded by a plate reader (560 nm excitation, 590 nm emission).

MTT assay. U87 cells treated with different concentrations of digitonin were seeded in the 96-well plate and incubated over- night. 10 μL of 12 mM MTT/PBS solution was added to

each well and the plate was incubated at 37 °C for 4 hours. The absorbance values at 570 nm were recorded using a plate reader.

Cell number counting. Cells were seeded in a 96-well plate, and different concentrations of digitonin were added. The cell numbers were counted using a hemocytometer after a 2-day incubation.

Confocal imaging

Evaluating digitonin treatment results. Cells were loaded with the AKT cyclic peptide probes (Rhodamine-cy(GSQTH), 2 μM in MEB; Cy5-cy(YYTYT), 30 μM in MEB) using the digitonin treatment approach described above. Cells were then loaded on the microwell chip and imaged using a confocal microscope (Zeiss 880) following established protocols.

Single-cell monitoring of AKT signaling activities. THP-1 cells and Jurkat cells were loaded onto the microwell chip at a concentration of 800 k mL^{-1} and incubated at 37 °C. Extra cells were scraped off the chip surface, and the chip was washed with fresh cell culture media. The cells were imaged using a confocal microscope (Zeiss 880) following established protocols. AZD8055 was introduced to reach final concentrations of 1 μM (THP-1) and 0.5 μM (Jurkat) during the experiments.

Immunofluorescence

The cells were fixed with cold methanol (−20 °C) on the chip right after the confocal imaging. Five minutes later, the chip was washed with PBS (5 minutes × 3 times). After fixation, the chip loaded with cells was blocked by goat serum at room temperature for an hour. The AKT detection antibody solution was prepared by mixing 3.8 μL of AKT antibody solution (as purchased, Cell Signaling Technology #5186) and 1 mL of 1% BSA

in PBS. The cells were incubated with the detection anti- body solution on the chip at 4 °C overnight. After incubation, the chip was washed with PBS and then imaged using the confocal microscope (Zeiss 880).

Single-cell data analysis

Data extraction. The obtained single-cell image stacks were analyzed using Fiji following established protocols. The FRET signal intensities from every single cell were plotted to generate single-cell AKT signaling trajectories. The AKT expression levels were obtained from extracting the fluorescence intensities from each single cell after the immunostaining.

DTW analysis. Pairwise dynamic time warping analysis was performed using the dtw function in MATLAB®. The result was presented as a distance matrix, where each matrix element rep- resented the dissimilarity between two single-cell trajectories.

AHC analysis. The clustering was performed with the Hierarchical Cluster Analysis tool in OriginPro®2019b. The clusters were identified based on the Euclidean distances between elements and Ward's method. The result was a dendrogram showing different clusters in the dataset. This dendrogram was then combined with the heatmap generated from the DTW analysis to highlight the clusters.

Mann–Whitney test. The AKT expression level distributions from the three clusters were evaluated using the Mann– Whitney test. This analysis was performed in OriginPro®2019b.

3.3 Results and Discussion

Digitonin treatment on U87 cells

Digitonin is known to cause membrane perforation, which may lead to cell damage. Therefore, it is critical to optimize its concentration so that cells are not significantly harmed. We first evaluated the effect of digitonin on U87 cells, which were used extensively in our previous studies. Interestingly, we observed that 1 μg mL^{-1} digitonin treatment led to a slight increase in cell viability and metabolic activities, as evidenced by the elevated resazurin assay and MTT assay values (Fig. 3.2a and b). Raising the digitonin concentration to 3 μg mL^{-1} diminished the pro-growth effects and led to indistinguishable viability values as those from the control samples. Further increasing the digitonin concentration to 5 μg mL^{-1} caused inhibition of the cell viability, indicating significant toxicity to the cells. Because our goal is to continuously analyze AKT signaling activities in living cells, it is paramount not to substantially alter cell viability. Therefore, it was evident that 5 μg mL^{-1} was not acceptable for our purpose. Nevertheless, it is worth pointing out that 5 μg mL^{-1} was a commonly used digitonin concentration in the literature, especially those involving the delivery of large molecules. In those studies, the main goal was to perform the delivery instead of performing analysis.[30–32] Thus, the requirements are different here, and we must use lower digitonin concentrations to avoid cytotoxicity.

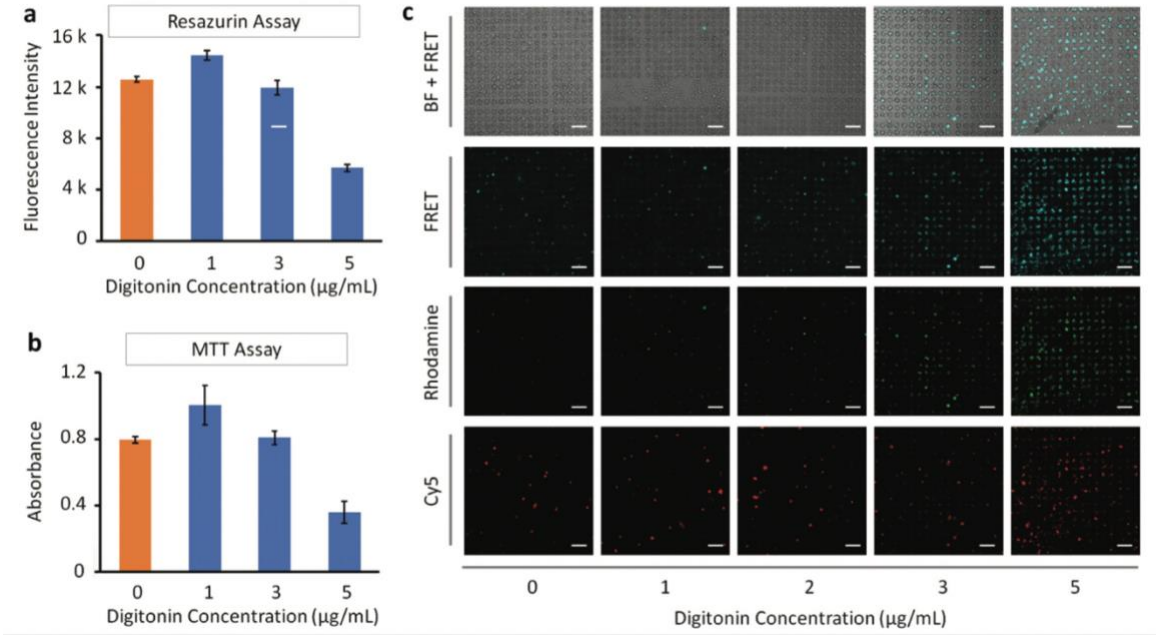

Fig. 3.2 The effect of digitonin treatment on U87 cells. (**a**) Resazurin assay and (**b**) MTT assay results were used to evaluate cell viability. (**c**) Confocal images of U87 cells treated with different concentrations of digitonin and loaded with the peptide probes. Cells were placed on a microwell chip to facilitate the imaging. Scale bars: 100 µm. Microwell chips with different well diameters were used for the samples.

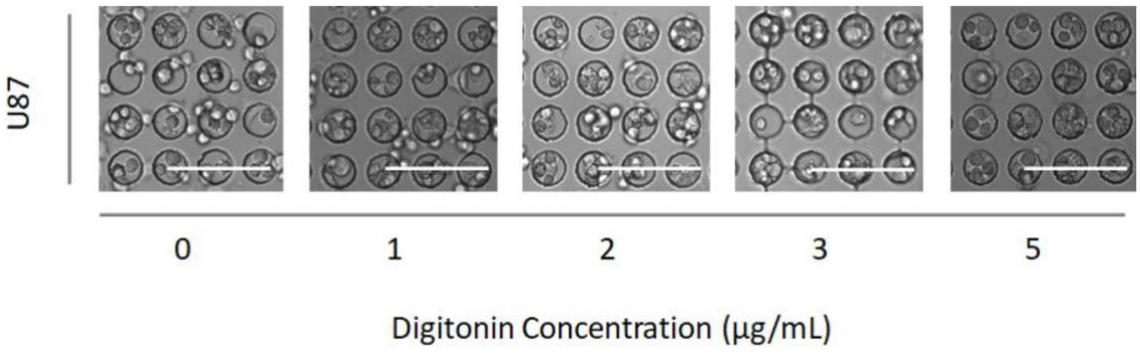

Fig. 3.3 Zoom-in images of the U87 cells treated with digitonin. Scale bar: 100 µm.

We then sought to check if digitonin treatment could indeed allow cyclic peptide probes to diffuse across the cell membrane. We treated the U87 single-cell suspension with varying concentrations of digitonin in the presence of our cyclic peptide probes, Rhodamine-cy(GSQTH) and Cy5-cy(YYTYT). After incubation and washing the cells, we loaded the cells into a microwell chip following established protocols and used a confocal microscope to evaluate the intracellular fluorescence signal. As shown in Fig. 3.2c, increasing digitonin concentrations led to elevating intracellular fluorescence intensities. This result is consistent with our expectation that higher digitonin concentrations would better facilitate the diffusion of cyclic peptide probes across the cell membrane. In addition, digitonin treatment did not alter the morphology of the cells (Fig. 3.3). Taken together, 2 or 3 μg mL^{-1} turned out to be suitable digitonin concentrations for U87 cells.

Digitonin treatment on THP-1 cells

Since U87 cells are genuinely adherent cells, their properties are different from those true suspension cells such as myeloid and lymphoid cells. In order to test if digitonin would work on genuine suspension cells, we moved on to perform the experiments using THP-1 cells. These monocytic cells are of the myeloid lineage and are representative suspension cells.[33,34] We first treated these THP-1 cells with varying concentrations of digitonin and evaluated the cell viability using the resazurin assay. As shown in Fig. 3.4a, all the tested digitonin concentrations led to lowered fluorescence signals compared with the control. This result indicated that THP-1 cells were more sensitive to digitonin treatment than U87 cells.

Nevertheless, because THP-1 cells may alter their metabolic pattern under external stimulation,[35,36] the resazurin test result could not directly translate to cell viability. To better access cell viability, we resorted to cell counting. We treated THP-1 cells with different concentrations of digitonin and then incubated the cells for two days. We then counted the viable cells in each sample (Fig. 3.4b). Interestingly, we found that 1 μg mL^{-1} digitonin treatment promoted cell growth, and 2 μg mL^{-1} digitonin exhibited the same cell number as control. Higher digitonin concentrations (3 and 4 μg mL^{-1}) obviously inhibited cell proliferation, indicating that these concentrations caused substantial damage to the cells. This result was very similar to that from the U87 experiments but underscored that THP-1 cells were more prone to digitonin- induced metabolic alterations than U87 cells.

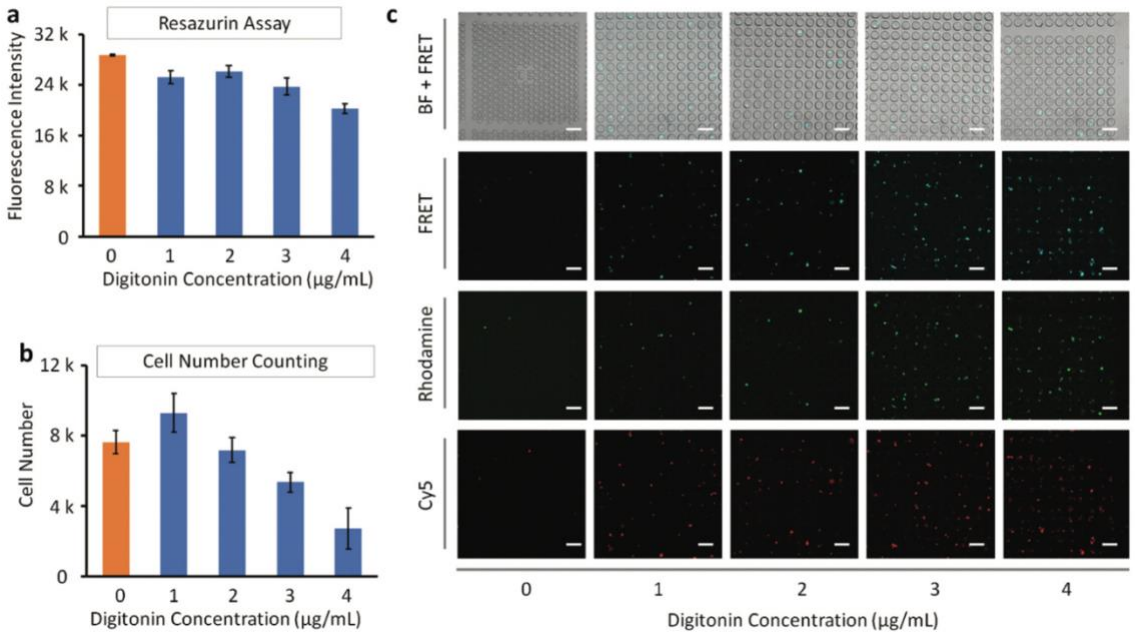

Fig. 3.4 The effect of digitonin treatment on THP-1 cells. (**a**) Resazurin assay and (**b**) cell counting assay results were used to evaluate cell viability. (**c**) Confocal images of THP-1 cells treated with digitonin and loaded with the peptide probes. Cells were placed on a microwell chip to facilitate the imaging. Scale bars: 100 μm. Microwell chips with different well diameters were used for the samples.

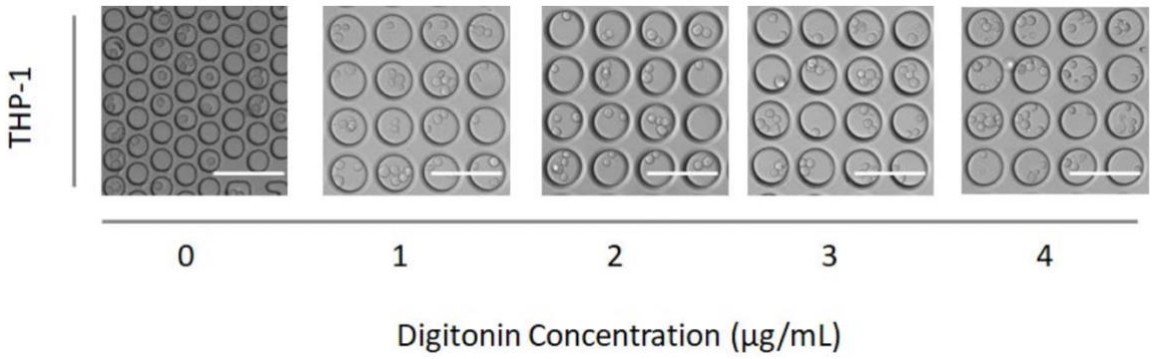

Fig. 3.5 Zoom-in images of the THP-1 cells treated with digitonin. Scale bar: 100 μm. Different sized microwells were used in the experiment.

To evaluate if digitonin could also enable cyclic peptides to move across the THP-1 cell membrane, we co-treated these cells with digitonin and the peptide probes. We then loaded the cells onto the microwell chip, and performed confocal microscopy. We found that even 1 μg mL^{-1} of digitonin led to a substantial amount of cyclic peptide probes present in the cells (Fig. 3.4c). With increasing digitonin concentrations, the intracellular FRET signals also increased. This trend was consistent with our expectations and was similar to what we observed in the U87 experiments. Considering the cell viability results above (Fig. 3.4b), we reasoned that 2 μg mL^{-1} of digitonin was suitable for treating THP-1 cells.

THP-1 cells are sensitive to external stimuli and prone to differentiating into macrophage-like phenotypes (M1 and M2),[34] their cell morphology can serve as an additional parameter for evaluating the effects of digitonin treatment. Based on our observation (Fig. 3.5), 1–4 μg mL^{-1} digitonin did not alter cell morphology, indicating that these concentrations did not cause phenotypical changes, which further validated the suitability of our approach.

Digitonin treatment on Jurkat cells

We then set to test if the digitonin approach was suitable for lymphoid cells, using Jurkat cells as a model system. Jurkat cells are immortalized human T lymphocytes, which are widely used in biomedical studies because of their close resemblance to normal T cells.[37] Similar to the THP-1 experiments, we first treated Jurkat cells with 1–4 μg mL^{-1} of digitonin and assessed its effect on cell viability using the resazurin assay. We found that digitonin treatment caused significantly lower metabolic activities, and this inhibition effect became more prominent with increasing digitonin concentrations (Fig. 3.6a). Because Jurkat cells were also sensitive to external perturbations and could alter their metabolic patterns in response to digitonin treatments,[38,39] it was again necessary to validate our findings using cell counting. We treated the Jurkat cells with different concentrations of digitonin, incubated the cells for two days, and then counted the viable cells. Our results showed that cell proliferation was not inhibited by the digitonin treatment (Fig. 3.6b). Interestingly, we did not observe the pro-proliferation effects of 1 μg mL^{-1} digitonin treatment, like those in the U87 and THP-1 experiments. Based on these results, we concluded that 2 μg mL^{-1} of digitonin was suitable for treating Jurkat cells.

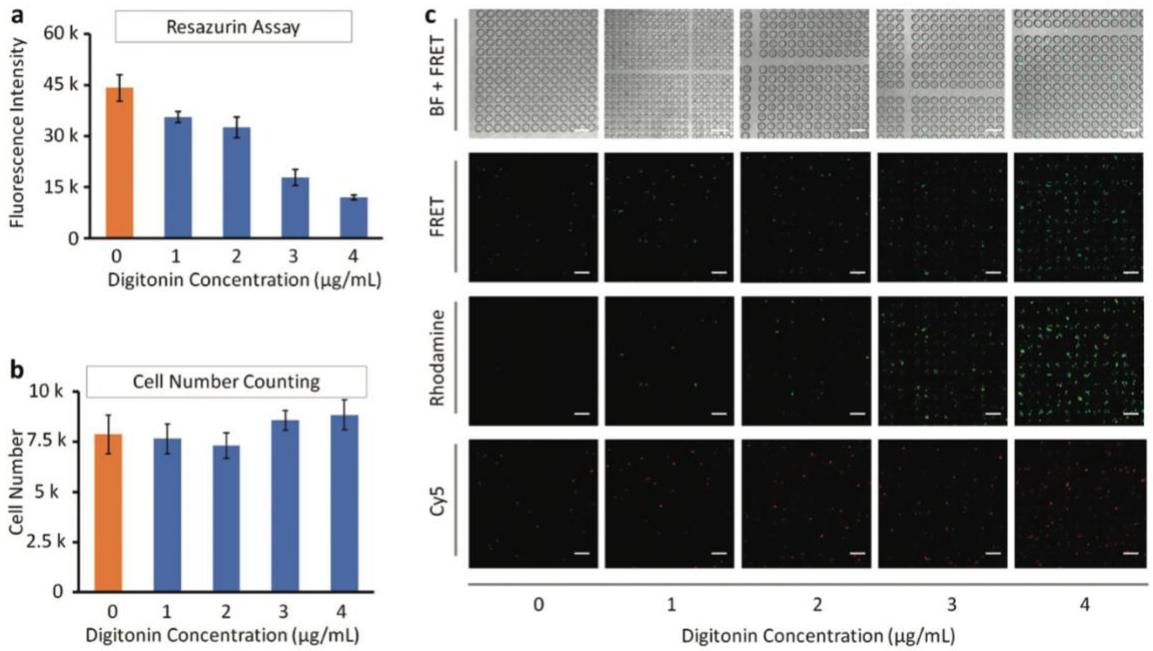

Fig. 3.6 The effect of digitonin treatment on Jurkat cells. (**a**) Resazurin assay and (**b**) cell counting assay results were used to evaluate cell viability. (**c**) Confocal images of Jurkat cells treated with digitonin and loaded with the peptide probes. Cells were placed on a microwell chip to facilitate the imaging. Scale bars: 100 μm. Microwell chips with different well diameters were used for the samples.

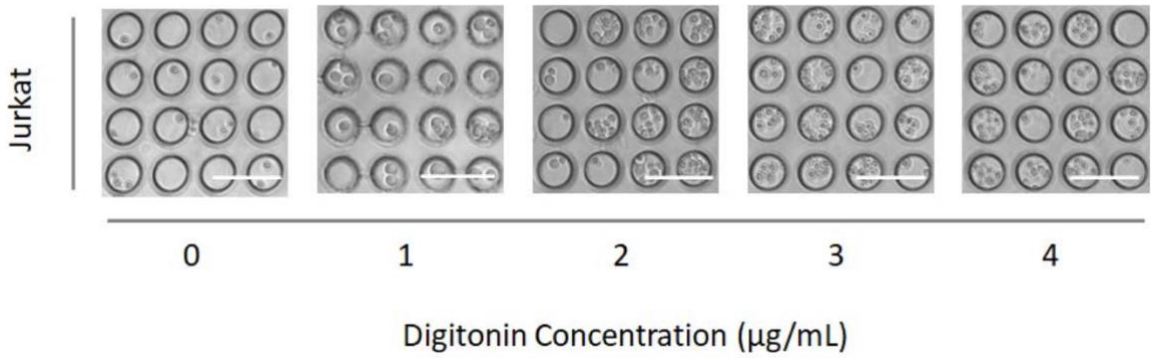

Fig. 3.7 Zoom-in images of the Jurkat cells treated with digitonin. Scale bar: 100 μm. Different sized microwells were used in the experiment.

To assess the performance of the digitonin approach in delivering cyclic peptide probes into Jurkat cells, we incubated the cells in the presence of digitonin and the peptide probes and performed the confocal microscopy experiments as described above. We found that higher digitonin concentrations led to more intense FRET signals across the cell populations, which was consistent with the results from U87 and THP-1 experiments (Fig. 3.6c). We also observed substantial levels of FRET signals in samples treated with digitonin at low concentrations (1 and 2 μg mL^{-1}). In addition, no morphological changes were observed (Fig. 3.7). Taken together, our results proved that digitonin treatment was an effective method for delivering cyclic peptide probes into Jurkat cells.

Single-cell profiling of AKT signaling activities in THP-1 cells

To further assess the performance of the digitonin approach, we delivered the cyclic peptide probes into THP-1 cells and performed continuous interrogation of the AKT signaling activities (Fig. 3.8a). Based on our results above, we chose 2 μg mL^{-1} as the optimal digitonin concentration. After incubating the cells with the peptide probes, we loaded the cells onto the microwell chip at a low concentration to achieve single-cell segregation. We then continuously monitored the FRET signals in those cells using confocal microscopy. During the imaging sessions, we added AZD8055 (an mTOR inhibitor) to the media to perturb the AKT signaling. At the end of the experiments, we fixed the cells in the microwells and performed immunofluorescence staining using an AKT antibody tagged with Alexa Fluor 647. The same cells were then imaged again to obtain the AKT immunofluorescence data.

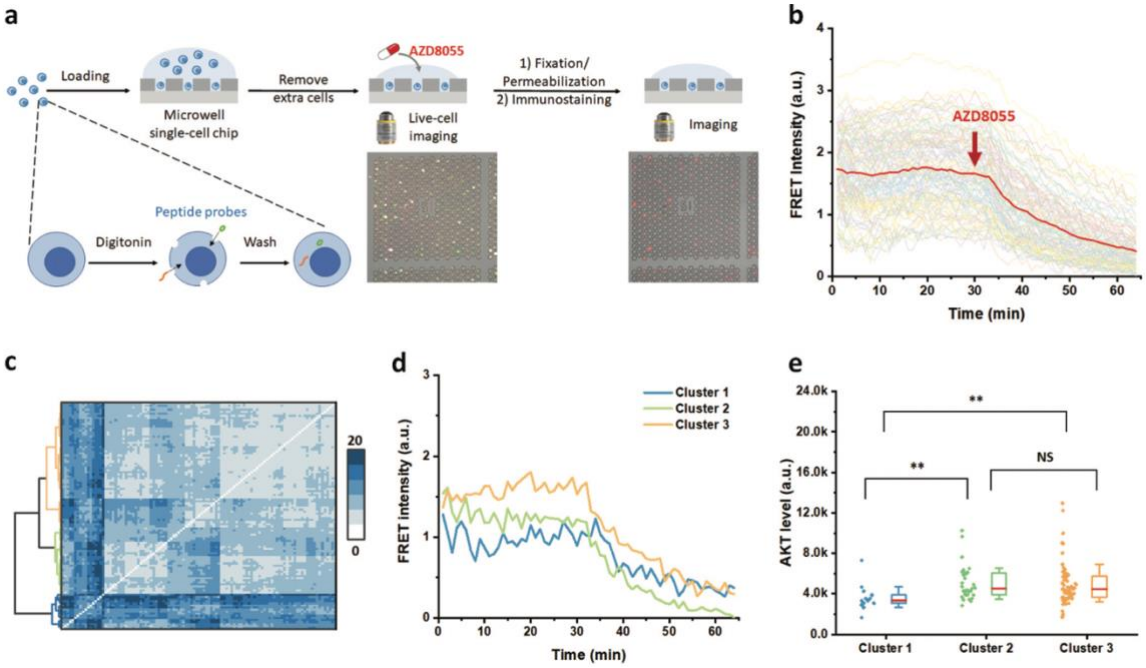

Fig. 3.8 (**a**) Schematic illustration of the experiment process. THP-1 cells were first treated with digitonin to allow peptide probes to diffuse into the cytosol. After washing and sealing the cells, the probe-loaded cells were placed on a microwell single-cell chip, where cells sank to the bottom of the wells. Continuous live-cell confocal imaging allowed monitoring AKT signaling activities from the single cells, and subsequent immunofluorescence staining enabled quantitation of AKT expression levels from the same set of single cells. (**b**) The single-cell AKT signaling trajectories generated by extracting signal intensities from the time-resolved image stacks. Each thin trace represents a single cell. The bold red trace represents the average activities from all the monitored single cells. (**c**) Agglomerative hierarchical clustering results generated from the dynamic time warping distance (DTW) matrix. Three distinct clusters were identified. The intensity of each pixel represents the corresponding DTW distance between two single cells. (**d**) AKT signaling patterns of the cluster centroids. (**e**) AKT expression levels obtained from the immunofluorescence staining results. The red horizontal lines represent the median levels in each cluster. The boxes denote the middle two quartiles, and the whiskers represent the standard deviation of each distribution. Mann–Whitney tests were used to compare the distributions. **: $p < 0.01$. NS: not significant.

The image stacks obtained from the live-cell imaging sessions contained the information of time-resolved AKT signal- ling activities at single-cell resolution. As shown in Fig. 3.8b, THP-1 cells exhibited fluctuating AKT activities before the drug addition, while the average signal levels among all the cells remained stable. This result was expected because the bulk- level AKT activity should not change significantly without external stimuli. Upon introducing the mTOR inhibitor (AZD8055), the average AKT activities gradually decreased. Since mTOR inhibition would cause de-phosphorylation of AKT at Ser473/474, the observed signal decrease was consistent with the mechanism of action. Notably, there was significant heterogeneity in the levels and rates of the signal decrease.

To better evaluate the cellular heterogeneity and to quantitatively compare the kinetic patterns of AKT signaling activities, we used the dynamic time warping (DTW) approach to analyze the time-resolved single-cell dataset. The DTW method was developed to evaluate the similarities in the time-evolution trends of signals without interference from speed variations. By performing pairwise DTW analysis,[41,42] we converted the single-cell trajectories (Fig. 3.8b) into a distance matrix, where each matrix element represented the dissimilarities between a pair of single cells (Fig. 3.9). Using this distance matrix, we were able to implement an agglomerative hierarchical clustering (AHC) strategy to identify subpopulations among the single cells. As shown in Fig. 3.8c, there were three distinct sub-populations (Fig. 3.10 and 3.11). As represented by the cluster centroids (Fig. 3.8d), each cluster displayed unique AKT signaling patterns. Cluster 1 cells exhibited strong fluctuations at basal condition, and relatively small responses to the drug perturbation. Cluster 2 cells and cluster 3 cells had similar drug responses, but cluster 2 cells displayed

gradually decreasing AKT signaling activities at the basal condition, while cluster 3 cells had slightly increasing AKT activities before drug addition (Fig. 3.11).

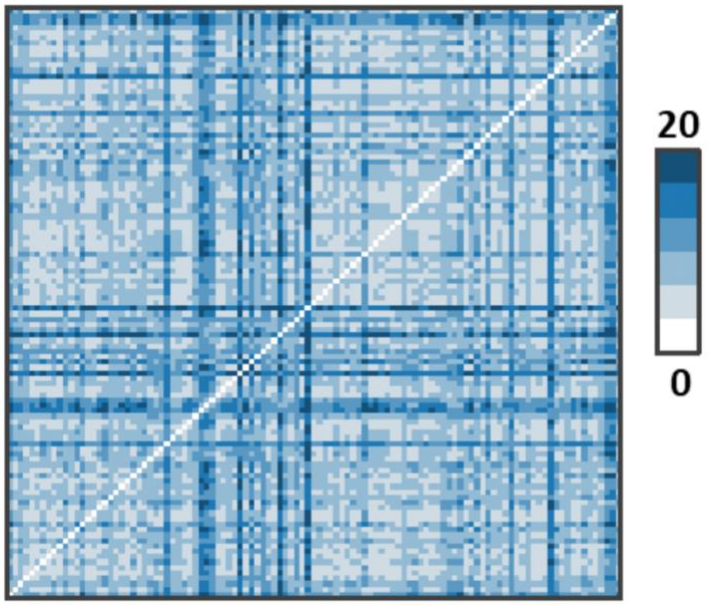

Fig. 3.9 The distance matrix generated from the DTW analysis on the THP-1 data set. Each pixel represents the dissimilarity between two corresponding single cells (column and row).

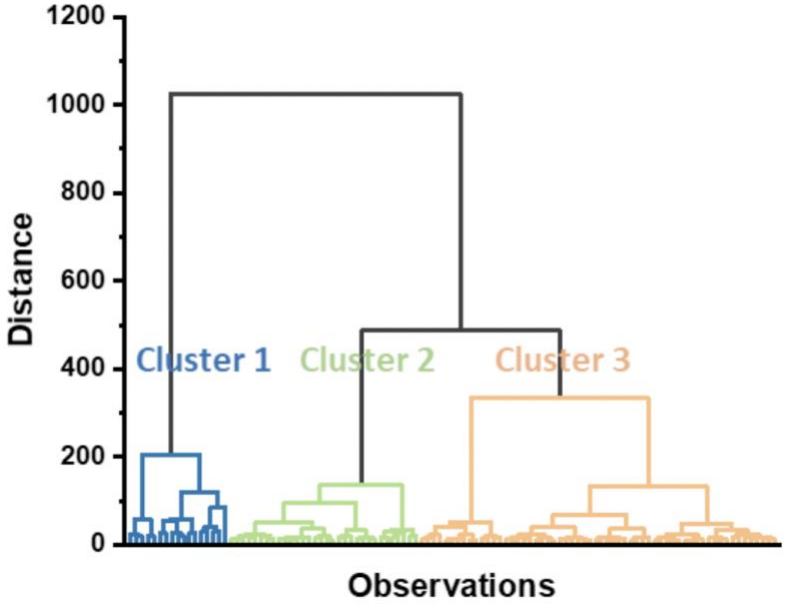

Fig. 3.10 Agglomerative hierachical clustering results of the distance matrix (THP-1 cells).

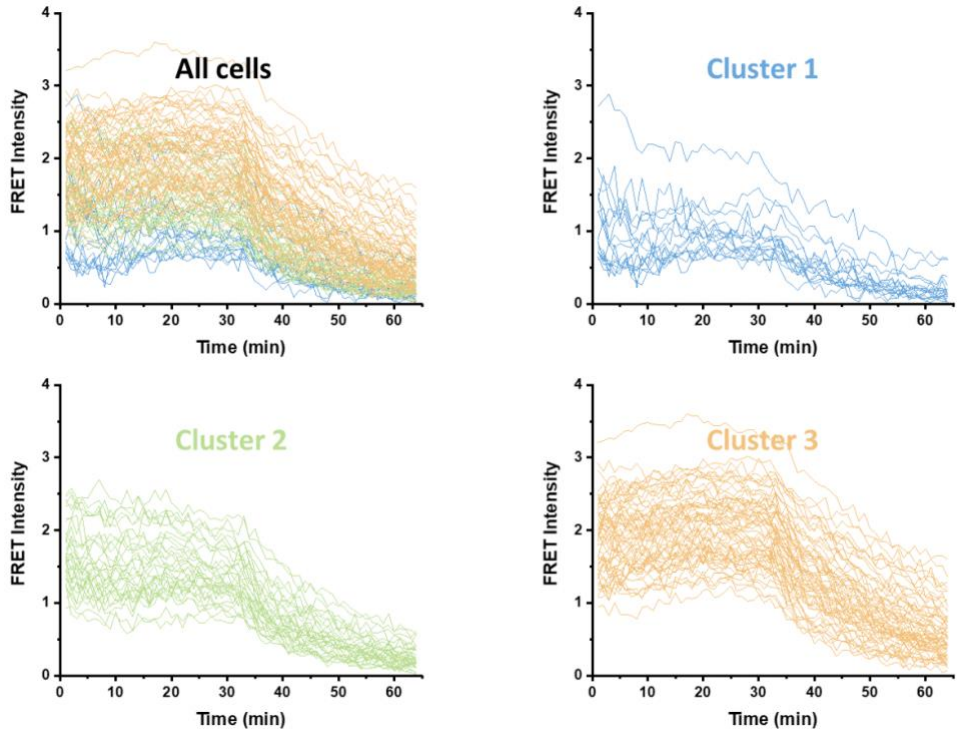

Fig. 3.11 Single-cell AKT signaling trajectories. The clusters are color-coded (THP-1 cells).

Because we were able to perform immunofluorescence staining on the same set of single cells, we could test if AKT expression levels varied among those three clusters. We extracted the AKT levels from all single cell and categorized them according to the cluster designations. We then used the Mann– Whitney test to compare the distributions among the three sub- populations. As shown in Fig. 3.8e, there were no statistically significant differences between clusters 2 and 3, while cluster 1 cells exhibited significantly lower AKT expression levels. This result suggested that AKT expression levels may affect the kinetic patterns of AKT signaling activities in THP-1 cells. In addition, lower AKT expression levels may link to more intense baseline fluctuations and less sensitivity to mTOR inhibition.

Single-cell profiling of AKT signaling activities in Jurkat cells

To test the generalizability of the digitonin approach, as well as the observed connection between AKT expression levels and AKT signaling patterns, we performed similar experiments using Jurkat cells. As shown in Fig. 3.12a, at basal condition, Jurkat cells exhibited much higher heterogeneity in AKT sig- nalling activity levels compared with THP-1 cells. This result was expected because Jurkat cells were known to be highly heterogeneous.[40] Upon mTOR inhibition, the AKT signaling levels decreased gradually. On average, the signal decreased by 40% in 10 min, consistent with the results from THP-1 cells. Interestingly, some cells exhibited transient signal increase immediately after the mTOR inhibitor addition. Using pairwise DTW and AHC analysis, we identified three subpopulations among the Jurkat cells (Fig. 3.12b and Fig. 3.13, 3.14). Notably, each clusters had unique features (Fig. 3.12c and Fig. 3.15). Cluster 1 cells displayed quick dips immediately after drug addition, followed by pronounced signal decrease over the time course. Cluster 2 cells showed slight jumps immediately after the drug addition, followed by prominent signal decrease. Cluster 3 cells exhibited much stronger jumps after drug addition, and their overall signal decrease over the time course were much smaller compared with the other two clusters. Surprisingly, the AKT expression levels did not vary significantly across these three clusters. This result indicated that the kinetic patterns of AKT signaling decoupled from the AKT expression levels in Jurkat cells.

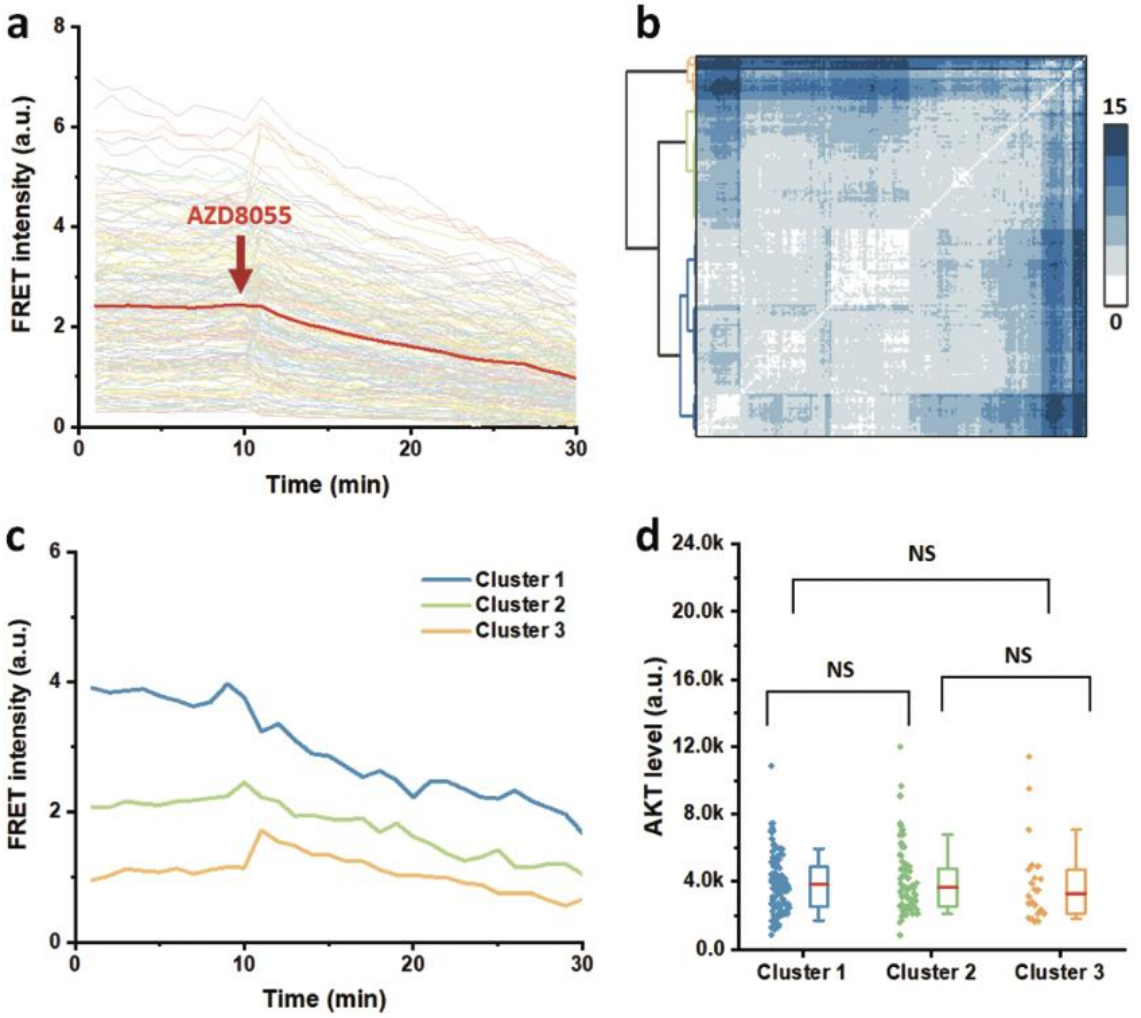

Fig. 3.12 Single-cell profiling of AKT signaling activities in Jurkat cells (**a**) The single-cell AKT signaling trajectories of Jurkat cells. Each thin trace represents a single cell. The bold red trace represents the average activities from all the monitored single cells. (**b**) Agglomerative hierarchical clustering results generated from the DTW matrix. Three distinct clusters were identified. The intensity of each pixel represents the corresponding DTW distance between two single cells. (**c**) AKT signaling patterns of the cluster centroids. (**d**) AKT expression levels obtained from the immunofluorescence staining results. The red horizontal lines represent the median levels in each cluster. The boxes denote the middle two quartiles, and the whiskers represent the standard deviation of each distribution. Mann–Whitney tests were used to compare the distributions. NS: not significant.

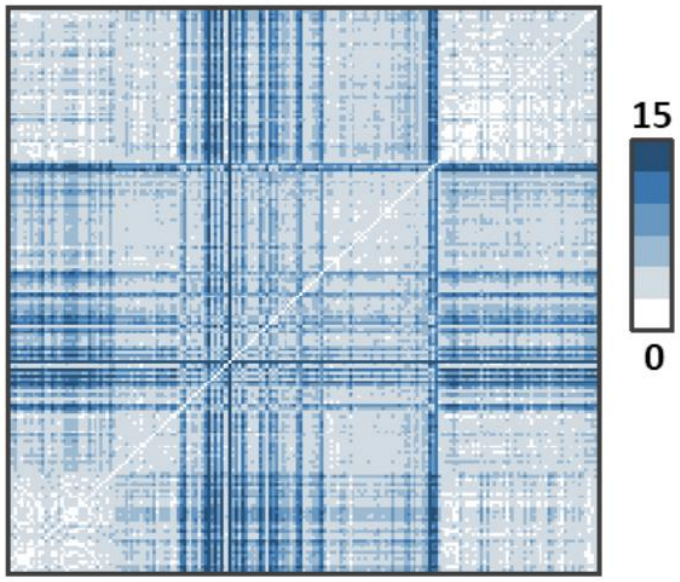

Fig. 3.13 The distance matrix generated from the DTW analysis on the Jurkat data set. Each pixel represents the dissimilarity between two corresponding single cells (column and row).

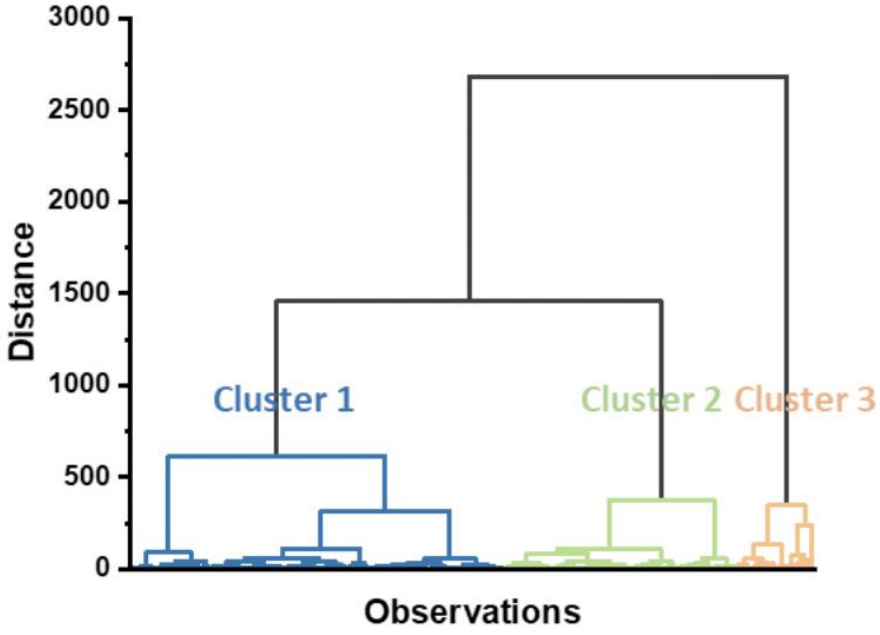

Fig. 3.14 Agglomerative hierachical clustering results of the distance matrix (Jurkat cells).

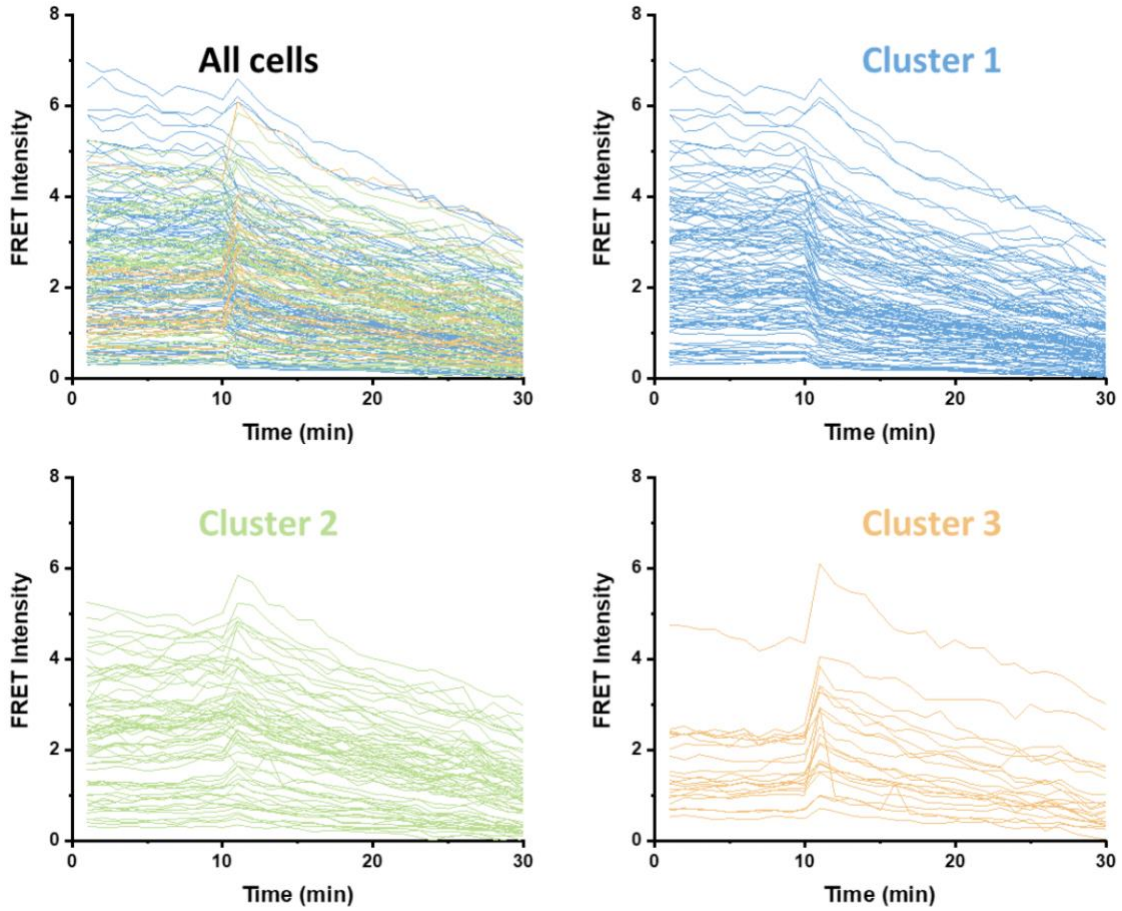

Fig. 3.15 Single-cell AKT signaling trajectories. The clusters are color-coded (Jurkat cells).

3.4 Conclusions

In conclusion, we have established a method for delivering cyclic peptide-based imaging probes into suspension cells using digitonin. At low concentrations (1–2 μg mL^{-1}), digitonin was not toxic to the cells but was able to transiently permeabilize the plasma membrane, which allowed the diffusion of peptide probes into the cytosol. We showed that this digitonin strategy was applicable to various cell types, such as single-cell suspension of genuinely adherent cells (U87), myeloid cells (THP-1), and lymphoid cells (Jurkat).

Using the digitonin delivery method, we further demonstrated the analysis of AKT signaling activities in THP-1 and Jurkat cells, followed by the immunofluorescence quantitation of AKT expression levels. With these datasets, we showed that under mTOR inhibition, the kinetic features of AKT signaling activities and the AKT expression levels were related in THP-1 cells, but are decoupled in Jurkat cells. Our results showcased the application of our strategy, underscored the AKT signaling heterogeneity in different cell lines, and highlighted how such an analytical workflow led to a better understanding of the single-cell AKT signaling dynamics.

3.5 References

1. Lim, J. S.; Ibaseta, A.; Fischer, M. M.; Cancilla, B.; O'Young, G.; Cristea, S.; Luca, V. C.; Yang, D.; Jahchan, N. S.; Hamard, C.; Antoine, M.; Wislez, M.; Kong, C.; Cain, J.; Liu, Y. W.; Kapoun, A. M.; Garcia, K. C.; Hoey, T.; Murriel, C. L.; Sage, J., Intratumoural heterogeneity generated by Notch signalling promotes small-cell lung cancer. *Nature* **2017,** *545* (7654), 360-364.

2. Welch, D. R., Tumor Heterogeneity—A 'Contemporary Concept' Founded on Historical Insights and Predictions. *Cancer Research* **2016,** *76* (1), 4.

3. Wei, W.; Shin, Y. S.; Xue, M.; Matsutani, T.; Masui, K.; Yang, H.; Ikegami, S.; Gu, Y.; Herrmann, K.; Johnson, D.; Ding, X.; Hwang, K.; Kim, J.; Zhou, J.; Su, Y.; Li, X.; Bonetti, B.; Chopra, R.; James, C. D.; Cavenee, W. K.; Cloughesy, T. F.; Mischel, P. S.; Heath, J. R.; Gini, B., Single-Cell Phosphoproteomics Resolves Adaptive Signaling Dynamics and Informs Targeted Combination Therapy in Glioblastoma. *Cancer Cell* **2016,** *29* (4), 563-573.

4. Xue, M.; Wei, W.; Su, Y.; Kim, J.; Shin, Y. S.; Mai, W. X.; Nathanson, D. A.; Heath, J. R., Chemical Methods for the Simultaneous Quantitation of Metabolites and Proteins from Single Cells. *Journal of the American Chemical Society* **2015,** *137* (12), 4066-4069.

5. Pisco, A. O.; Huang, S., Non-genetic cancer cell plasticity and therapy-induced stemness in tumour relapse: 'What does not kill me strengthens me'. *British Journal Of Cancer* **2015,** *112*, 1725.

6. Pisco, A. O.; Brock, A.; Zhou, J.; Moor, A.; Mojtahedi, M.; Jackson, D.; Huang, S., Non-Darwinian dynamics in therapy-induced cancer drug resistance. *Nature communications* **2013,** *4*, 2467.

7. Su, Y.; Wei, W.; Robert, L.; Xue, M.; Tsoi, J.; Garcia-Diaz, A.; Homet Moreno, B.; Kim, J.; Ng, R. H.; Lee, J. W.; Koya, R. C.; Comin-Anduix, B.; Graeber, T. G.; Ribas, A.; Heath, J. R., Single-cell analysis resolves the cell state transition and signaling dynamics associated with melanoma drug-induced resistance. *Proceedings of the National Academy of Sciences* **2017,** *114* (52), 13679.

8. Shaffer, S. M.; Dunagin, M. C.; Torborg, S. R.; Torre, E. A.; Emert, B.; Krepler, C.; Beqiri, M.; Sproesser, K.; Brafford, P. A.; Xiao, M.; Eggan, E.; Anastopoulos, I. N.; Vargas-Garcia, C. A.; Singh, A.; Nathanson, K. L.; Herlyn, M.; Raj, A., Rare cell variability and drug-induced reprogramming as a mode of cancer drug resistance. *Nature* **2017,** *546*, 431.

9. Andrews, S. S.; Peria, W. J.; Yu, R. C.; Colman-Lerner, A.; Brent, R., Push-Pull and Feedback Mechanisms Can Align Signaling System Outputs with Inputs. *Cell Systems* **2016,** *3* (5), 444-455.e2.

10. Artyomov, M. N.; Das, J.; Kardar, M.; Chakraborty, A. K., Purely stochastic binary decisions in cell signaling models without underlying deterministic bistabilities. *Proceedings of the National Academy of Sciences* **2007,** *104* (48), 18958.

11. Santos, S. D. M.; Verveer, P. J.; Bastiaens, P. I. H., Growth factor-induced MAPK network topology shapes Erk response determining PC-12 cell fate. *Nature Cell Biology* **2007,** *9*, 324.

12. Ting, A. Y.; Kain, K. H.; Klemke, R. L.; Tsien, R. Y., Genetically encoded fluorescent reporters of protein tyrosine kinase activities in living cells. *Proceedings of the National Academy of Sciences* **2001,** *98* (26), 15003.

13. Oldach, L.; Zhang, J., Genetically Encoded Fluorescent Biosensors for Live-Cell Visualization of Protein Phosphorylation. *Cell Chem. Biol.* **2014,** *21* (2), 186-197.

14. Sasaki, K.; Sato, M.; Umezawa, Y., Fluorescent Indicators for Akt/Protein Kinase B and Dynamics of Akt Activity Visualized in Living Cells. *Journal of Biological Chemistry* **2003,** *278* (33), 30945-30951.

15. Kunkel, M. T.; Ni, Q.; Tsien, R. Y.; Zhang, J.; Newton, A. C., Spatio-temporal dynamics of protein kinase B/Akt signaling revealed by a genetically encoded fluorescent reporter. *The Journal of biological chemistry* **2005,** *280* (7), 5581-5587.

16. Gao, X.; Zhang, J., Spatiotemporal analysis of differential Akt regulation in plasma membrane microdomains. *Molecular biology of the cell* **2008,** *19* (10), 4366-4373.

17. Shao, S.; Li, Z.; Cheng, H.; Wang, S.; Perkins, N. G.; Sarkar, P.; Wei, W.; Xue, M., A Chemical Approach for Profiling Intracellular AKT Signaling Dynamics from Single Cells. *Journal of the American Chemical Society* **2018,** *140* (42), 13586-13589.

18. Gross, S. M.; Rotwein, P., Akt signaling dynamics in individual cells. *Journal of cell science* **2015,** *128* (14), 2509-2519.

19. Gao, X.; Zhang, J., Akt signaling dynamics in plasma membrane microdomains visualized by FRET-based reporters. *Communicative & integrative biology* **2009,** *2* (1), 32-34.

20. Heath, J. R.; Ribas, A.; Mischel, P. S., Single-cell analysis tools for drug discovery and development. *Nature Reviews Drug Discovery* **2016,** *15* (3), 204-216.

21. Ignatiadis, M.; Sledge, G. W.; Jeffrey, S. S., Liquid biopsy enters the clinic — implementation issues and future challenges. *Nature Reviews Clinical Oncology* **2021,** *18* (5), 297-312.

22. Schafflick, D.; Xu, C. A.; Hartlehnert, M.; Cole, M.; Schulte-Mecklenbeck, A.; Lautwein, T.; Wolbert, J.; Heming, M.; Meuth, S. G.; Kuhlmann, T.; Gross, C. C.; Wiendl, H.; Yosef, N.; Meyer zu Horste, G., Integrated single cell analysis of blood and cerebrospinal fluid leukocytes in multiple sclerosis. *Nature Communications* **2020,** *11* (1), 247.

23. Qian, Z.; Martyna, A.; Hard, R. L.; Wang, J.; Appiah-Kubi, G.; Coss, C.; Phelps, M. A.; Rossman, J. S.; Pei, D., Discovery and Mechanism of Highly Efficient Cyclic Cell-Penetrating Peptides. *Biochemistry* **2016,** *55* (18), 2601-2612.

24. Guidotti, G.; Brambilla, L.; Rossi, D., Cell-Penetrating Peptides: From Basic Research to Clinics. *Trends in Pharmacological Sciences* **2017,** *38* (4), 406-424.

25. Liu, D.; Wang, L.; Wang, Z.; Cuschieri, A., Magnetoporation and Magnetolysis of Cancer Cells via Carbon Nanotubes Induced by Rotating Magnetic Fields. *Nano Letters* **2012,** *12* (10), 5117-5121.

26. Helfield, B.; Chen, X.; Watkins, S. C.; Villanueva, F. S., Biophysical insight into mechanisms of sonoporation. *Proceedings of the National Academy of Sciences* **2016,** *113* (36), 9983.

27. Patskovsky, S.; Qi, M.; Meunier, M., Single point single-cell nanoparticle mediated pulsed laser optoporation. *Analyst* **2020,** *145* (2), 523-529.

28. Korchowiec, B.; Gorczyca, M.; Wojszko, K.; Janikowska, M.; Henry, M.; Rogalska, E., Impact of two different saponins on the organization of model lipid membranes. *Biochimica et Biophysica Acta (BBA) - Biomembranes* **2015,** *1848* (10, Part A), 1963-1973.

29. Lorent, J. H.; Quetin-Leclercq, J.; Mingeot-Leclercq, M.-P., The amphiphilic nature of saponins and their effects on artificial and biological membranes and potential consequences for red blood and cancer cells. *Organic & Biomolecular Chemistry* **2014,** *12* (44), 8803-8822.

30. Deng, J.; Carlson, N.; Takeyama, K.; Dal Cin, P.; Shipp, M.; Letai, A., BH3 Profiling Identifies Three Distinct Classes of Apoptotic Blocks to Predict Response to ABT-737 and Conventional Chemotherapeutic Agents. *Cancer Cell* **2007,** *12* (2), 171-185.

31. Mai, W. X.; Gosa, L.; Daniels, V. W.; Ta, L.; Tsang, J. E.; Higgins, B.; Gilmore, W. B.; Bayley, N. A.; Harati, M. D.; Lee, J. T.; Yong, W. H.; Kornblum, H. I.;

Bensinger, S. J.; Mischel, P. S.; Rao, P. N.; Clark, P. M.; Cloughesy, T. F.; Letai, A.; Nathanson, D. A., Cytoplasmic p53 couples oncogene-driven glucose metabolism to apoptosis and is a therapeutic target in glioblastoma. *Nature medicine* **2017,** *23* (11), 1342-1351.

32. Ryan, J.; Letai, A., BH3 Profiling in Whole Cells by Fluorimeter or FACS. *Methods (San Diego, Calif.)* **2013,** *61* (2), 156-164.

33. Bosshart, H.; Heinzelmann, M., THP-1 cells as a model for human monocytes. *Ann Transl Med* **2016,** *4* (21), 438-438.

34. Genin, M.; Clement, F.; Fattaccioli, A.; Raes, M.; Michiels, C., M1 and M2 macrophages derived from THP-1 cells differentially modulate the response of cancer cells to etoposide. *BMC Cancer* **2015,** *15* (1), 577.

35. Mussotter, F.; Potratz, S.; Budczies, J.; Luch, A.; Haase, A., A multi-omics analysis reveals metabolic reprogramming in THP-1 cells upon treatment with the contact allergen DNCB. *Toxicology and Applied Pharmacology* **2018,** *340*, 21-29.

36. Abuawad, A.; Mbadugha, C.; Ghaemmaghami, A. M.; Kim, D.-H., Metabolic characterisation of THP-1 macrophage polarisation using LC–MS-based metabolite profiling. *Metabolomics* **2020,** *16* (3), 33.

37. Abraham, R. T.; Weiss, A., Jurkat T cells and development of the T-cell receptor signalling paradigm. *Nature Reviews Immunology* **2004,** *4* (4), 301-308.

38. Fernández-Ramos, A. A.; Marchetti-Laurent, C.; Poindessous, V.; Antonio, S.; Petitgas, C.; Ceballos-Picot, I.; Laurent-Puig, P.; Bortoli, S.; Loriot, M.-A.; Pallet, N., A comprehensive characterization of the impact of mycophenolic acid on the metabolism of Jurkat T cells. *Scientific Reports* **2017,** *7* (1), 10550.

39. Liao, W.; Tan, G.; Zhu, Z.; Chen, Q.; Lou, Z.; Dong, X.; Zhang, W.; Pan, W.; Chai, Y., Combined Metabonomic and Quantitative Real-Time PCR Analyses Reveal Systems Metabolic Changes in Jurkat T-Cells Treated with HIV-1 Tat Protein. *Journal of Proteome Research* **2012,** *11* (11), 5109-5123.

40. Myers, C. S.; Rabiner, L. R., A Comparative Study of Several Dynamic Time-Warping Algorithms for Connected-Word Recognition. *Bell System Technical Journal* **1981,** *60* (7), 1389-1409.

41. Vaughan, N.; Gabrys, B., Comparing and Combining Time Series Trajectories Using Dynamic Time Warping. *Procedia Computer Science* **2016,** *96*, 465-474.

42. Snow, K.; Judd, W., Heterogeneity of a human T-lymphoblastoid cell line. *Experimental Cell Research* **1987,** *171* (2), 389-403.

Chapter 4: Hydroxyl-rich endocytosis-promoting peptides

4.1 Introduction

Transporting cargo molecules into the cell is a critical and everlasting goal for many medicinal chemistry and chemical biology studies.[1, 2] As the natural route to bring molecules into the cell, the endocytosis process has been a primary focus in the field, especially when hydrophilic cargo molecules are involved.[3-5] A broad spectrum of endocytosis-promoting modalities has been discovered and developed[6, 7]. On the one hand, various nanoparticles, such as liposomes and micelles, can serve as delivery vehicles and bring native-state cargo molecules across the cell membrane.[8, 9] Some nanoparticle delivery platforms have already demonstrated clinical success.[10] On the other hand, smaller endocytosis-promoting moieties can be conjugated to cargo molecules and carry them into the cells.[11, 12] Compared with nanoparticle-based platforms, molecularly well-defined delivery tags allow for a more straightforward manufacturing process and a clearer path for medicinal chemistry optimizations. Representative examples of these molecularly well-defined groups include folate, transferrin, miniature proteins, and, notably, cell-penetrating peptides (CPPs).[13-17]

Over the past few decades, a very diverse panel of CPPs has been developed.[18] Early examples such as the transactivator of transcription (TAT) peptide and RGD sequence have proven capable of delivering various cargo molecules, and they continue to be widely employed to date.[19, 20] More recently, advanced sequences, such as penetratin, iRGD, and CPP12, have demonstrated superior delivery efficacy.[21-23] Currently, improving the cell-

penetrating ability, intracellular targeting, and biocompatibility of these CPPs remains a very active and attractive research field.[24-28]

Despite the prominent sequence variations, these CPPs share a common feature – they are positively charged.[29] This positive charge promotes the initial interaction with the extracellular matrix and the cell membrane, which is the prerequisite of endocytosis.[30] Consequently, the current dogma regards this positive charge as an indispensable component of CPPs.[17, 31, 32] Nevertheless, considering that even heavily negatively charged nanoparticles can still be taken up by the cells efficiently,[33] one may question the necessity of relying on positive charges to induce endocytosis. Herein, we present a series of endocytosis-promoting peptides (EPPs) that do not have positive charges. These cyclic peptides are rich in hydroxyl groups and can bring various cargo molecules into a diverse collection of cells.

4.2 Experimental

Materials

TentaGel S-NH_2 resin (loading capacity 0.28 mmol/g) was purchased from Rapp Polymere GmbH and Rink amide MBHA resin (loading capacity 0.678 mmol/g) from Aapptec (Louisville, KY). All the Fmoc-protected amino acids were purchased from Anaspec (Fremont, CA) except Fmoc-L-propargylglycine (Pra) and Fmoc- Lys(N_3)-OH (Az4), which were purchased from Chempep (Wellington, FL) and Chem-Impex (Wood Dale, IL), respectively. The coupling reagent 2-(1H-benzotriazol-1-yl)-1,1,3,3-tetramethyluronium hexafluorophosphate (HBTU, 99.6%) was obtained from Chem-Impex (Wood Dale, IL). Diisopropylethylamine (DIEA, 99.5%) was purchased from

ACROS (Germany). Phenyl isothiocyanate (PhNCS) and triisopropylsilane (TIPS) were obtained from TCI (Portland, OR). Piperidine was purchased from Alfa Aesar (Ward Hill, MA). 5(6)-carboxyfluorescein (Fluo) were obtained from ACROS (Pittsburg, PA). Rhodamine B (RB), cuprous iodide (CuI), and α-cyano-4-hydroxycinnamic acid (CHCA) were obtained from Sigma-Aldrich (St. Louis, MO). N, N′-dimethylformamide (DMF), and dichloromethane (DCM) were purchased from Thermo Fisher Scientific (Waltham, MA). Heparin sodium salt, porcine was purchased from MP Biomedicals (China). Cytochalasin D and Hydroxy Dynasore was bought from Tocris Bioscience (Bristol, United Kingdom). Phenothiazine was purchased from TCI (Portland, OR). Wortmannin was obtained from APExBIO Technology (Boston, MA). Pitstop 2 and filipin III was obtained from Sigma-Aldrich (St. Louis, MO). Methyl-beta-cyclodextrin was bought from Alfa Aesar (Haverhill, MA). Alexa Fluor 555 NHS ester and Alexa Fluor 647 NHS ester were purchased from Life Technologies (Eugene, OR). EGFP-Rab5, mEmerald-Caveolin-C-10, mEmerald-Clathrin-15 and mEmerald-Rab7a-7 were purchased from Addgene (Watertown, MA). The Caveolin-1 CRISPR/Cas9 KO plasmid, FIBCD1 CRISPR/Cas9 KO plasmid, control CRISPR plasmid were purchased from Santa Cruz Biotechnology (Santa Cruz, CA). ER-Tracker, Mito-Tracker and Lyso Tracker and all the antibodies were purchased from Cell Signaling Technology (Danvers, MA).

Preparative Reversed-Phase (RP) High-Performance Liquid Chromatography (HPLC)

Preparative HPLC was performed on a Thermo Ultimate 3000BX HPLC instrument, using a Phenomenex C18 reversed-phase preparative column (Kinetex 5 μm EVO, 250 × 21.2

mm^2). Nonlinear gradients of 0−100% acetonitrile (with 0.1% TFA) in water (with 0.1% TFA) were employed, and the gradient parameters were adjusted for each product to achieve desired separation efficiencies. A multiwavelength UV−vis detector was used to monitor the absorbance at 215, 280, 480, and 569 nm.

Analytical HPLC

The purity of the peptide was analyzed on a Thermo Ultimate 3000SD HPLC instrument, using a Phenomenex C18 reversed-phase analytical column (Kinetex 2.6 μm EVO, 250 × 4.6 mm^2). A gradient of 0−100% acetonitrile (with 0.1% TFA) in water (with 0.1% TFA) was employed with a flow rate of 1 mL/min. A UV−vis detector was used to monitor the absorbance at 280 or 560 nm. The purity of all cyclic peptides used for binding assays and biological activity assays was >95%.

Mass Spectrometry

The MS and MS/MS spectra were obtained using a SCIEX 5800 matrix-assisted laser desorption ionization time-of-flight (MALDI-TOF) mass spectrometer.

Solid-Phase Peptide Synthesis

The peptides were synthesized following the standard Fmoc SPPS coupling process. Unless otherwise noted, Rink Amide MBHA resin was used for the synthesis. To couple amino acids to the resin, the Fmoc group on the resin was first removed by 20% piperidine/DMF solution (10 min, three times). Fmoc-AA-OH (3 equiv), DIEA (5 equiv),

and HBTU (2.8 equiv) were mixed in DMF for 10 min, and the solution was then introduced to the deprotected resin. The mixture was gently agitated at room temperature for 1 h, followed by draining and washing (DMF, methanol, and DCM, three times each). To label the peptides with fluorophores, poly (ethylene glycol) (PEG), or biotin, the corresponding dye-COOH, Fmoc-PEG-OH, and biotin were coupled at the N-terminal using the SPPS procedure described above.

For constructing cyclic peptides, Fmoc-propargylglycine-OH (Pra) and Fmoc-azidolysine-OH (Az4) were inserted at the N and C terminals, respectively. A Cu-catalyzed click reaction was used for cyclization. Specifically, resins were incubated in 20% piperidine/ DMF with CuI (2.5 equiv) and L-ascorbic acid (5 equiv) at room temperature overnight. After cyclization, the beads were washed with sodium diethyldithiocarbamate (5% w/v) and DIEA (5% v/v) in DMF to remove the copper catalyst.

To cleave peptides off from the resin, a cleavage solution composed of TFA/TIPS/ddH2O (95:2.5:2.5) was used. The crude peptides were purified by preparative RP-HPLC, and the product purity and identity were confirmed by analytical RP-HPLC and mass spectrometry. RB-cy(YYTYT), $C_{79}H_{97}N_{14}O_{15}$+, $[M + H]^+$ calculated 1481.73, found 1481.62. RB-cy(TYYTY), $C_{79}H_{97}N_{14}O_{15}^+$, $[M + H]^+$ calculated 1481.73, found 1481.62. RB-cy(YTYYT), $C_{79}H_{97}N_{14}O_{15}^+$, $[M + H]^+$ calculated 1481.73, found 1481.74. RB-cy(YYYYY), $C_{89}H_{101}N_{14}O_{15}^+$, $[M + H]^+$ calculated 1605.76, found 1605.65. RB-cy(TTTTT), $C_{64}H_{91}N_{14}O_{15}^+$, $[M + H]^+$ calculated 1295.68, found 1295.62. RB-cy(YSYYS), $C_{77}H_{93}N_{14}O_{15}^+$, $[M + H]^+$ calculated 1453.69, found 1453.61. RB-cy(SYYSY),

$C_{77}H_{93}N_{14}O_{15}^{+}$, $[M + H]^{+}$ calculated 1453.69, found 145367. RB-cy(TAT), $C_{97}H1_{57}N_{36}O_{16}^{+}$, $[M + H]^{+}$ calculated 2082.26, found 2083.10. AF555-cy(YSYYS), $C_{71}H_{76}N_{14}O_{23}S_2^{2-}$, $[M + H]^{+}$ calculated 1556.47, found 1556.34. AF647-cy(YSYYS), $C_{89}H_{113}N_{14}O_{26}S_4^{3-}$, $[M + H]^{+}$ calculated 1921.68, found 1921.67. Fluo-cy(YSYYS), $C_{69}H_{72}N_{12}O_{19}$, $[M + H]^{+}$ calculated 1372.50, found 1372.25.

Cell lines and cell culture

The human glioblastoma cell line (U87) was gifted from Prof. Wei Wei (Institute For Systems Biology, Seattle). The human monocytic leukemia cell line (THP-1) and the human T-cell leukemia cell line (Jurkat) were purchased from ATCC. The human embryonic kidney cell line (HEK-293T), the human osteosarcoma cell line (U2OS), the human breast cancer cell line (MCF-7), the human metastatic melanoma cell lines (IGR-37, IGR-39, WM266-4 and WM115), the human cervical carcinoma cell line (HeLa), and the human myelogenous leukemia cell line (K562) were gifted from Prof. Yinsheng Wang (UC Riverside). The non-tumorigenic epithelial cell line (MCF 10A) and the human breast adenocarcinoma cell line (MDA-MB-231) were gifted from Prof. Wenwan Zhong (UC Riverside). The canine epithelial kidney cell line (MDCK) and the African green monkey kidney cell line (Vero) were gifted from Prof. Hai Rong (UC Riverside). The human colon carcinoma cell line (HCT116) was gifted from Prof. Xuan Liu (UC Riverside). The human liver carcinoma cell line (HEPG2), the rat liver cell line (MCA7777) and the mouse sarcoma cell line (J774A.1) were gifted from Prof. Joseph Genereux (UC Riverside).

For adherent cell lines, cells were cultured in Dulbecco's modified Eagle's medium (DMEM, Corning) supplemented with 10% heat-inactivated fetal bovine serum (FBS, Gibco) and 100 U/mL penicillin/streptomycin (Sigma). Cells were cultured under 5% CO_2 in a 37 °C incubator. A trypsin-EDTA solution (0.05%, Sigma) was used for passaging once the cells reached 80−90% confluency.

For suspension cell lines, cells were cultured in RPMI 1640, 1x (Corning) medium supplemented with 10% heat-inactivated fetal bovine serum (FBS, Gibco) and 100 U/mL penicillin/streptomycin (Sigma). Cells were cultured under 5% CO_2 in a 37 °C incubator. Fresh culture media was used to dilute old media at a 1:5 ratio after two doubling cycles.

Confocal Imaging experiments

To image the cells, a Zeiss 880 inverted confocal laser scanning microscope (Carl Zeiss, Germany) was used. Image acquisition and analyses were carried out using the manufacturer's software (ZEN, Carl Zeiss). Quantification of fluorescence intensity in single cells was performed using Fiji software.

Flow cytometry experiments

To measure the RB signal intensity, a NovoCyte flow cytometer (NovoExpress) was used. Quantification of fluorescence intensity in each condition was performed using Novoxpress software. Fifty thousand cells were analyzed for each condition. A green, fluorescent dye used in DNA staining, YOYO was included in all the flow cytometry experiments, serving as a cell live/dead indicator. For the YOYO only group, the cells were

treated with trypsin for 5-10 min. After that, cells were fixed in a 1.5 ml centrifuge tube using 4% paraformaldehyde at room temperature for 15 min. Subsequently, fixed cells were washed with PBS once and was permeabilized using 90% cold MeOH on ice for 15 min. Then, cells were incubated with YOYO in phenol-free medium. After half an hour, cells were centrifuged to get rid of YOYO solution and resuspended in fresh phenol-free medium before doing flow cytometry.

Dye-EPP incubation

For general incubation, 300 k U87 cells were seeded in full medium containing 10%FBS and 1% PS in a 35x10 mm petri dish. The cells were incubated overnight in full medium. Stock solution of Dye-EPPs were made in DMSO to reach a concentration of 500 μM. Fresh cell culture medium was used to dilute the stock solution to 500 nM and replace the old medium on day 2. Cells were incubated with RB-EPPs for different time periods, followed by a one-time wash with phenol-free fresh culture medium before measurements.

Concentration gradient experiment

U87 Cells were incubated with RB-EPP 6 at different concentrations (20 nM, 200 nM, 2 μM, 20 μM, 50 μM and 100 μM). After wash with fresh medium once cells were examined by confocal imaging.

Time series experiment

U87 Cells were incubated with RB-EPP 6 at 500 nM for 1 h. After wash with fresh medium once, the cells were kept in the 5% CO_2 incubator at 37 °C for different time durations (1 h, 2 h, 6 h and 24 h) before confocal imaging.

Temperature control comparison experiment

U87 cells were kept in the cold room for half an hour before incubated with RB-EPP 6. After that, cells were incubated with RB-EPP 6 at 500 nM at 4 °C. Cells in the control group were incubated at 37 °C. After 1 h, cells were wash with fresh medium once respectively before confocal imaging.

Endocytosis inhibitors treatment

U87 Cells were incubated with different endocytosis inhibitors for 1 h respectively. Afterwards, old medium was replaced with medium containing 500 nM RB-EPP 6. After 1 h, a trypsin-EDTA solution (0.05%, Sigma) was added to detach the cells. The cells were collected by centrifugation. Fresh phenol-free medium was added to each condition. Once resuspended, cells were filtered into glass tubes before flow cytometry.

Organelle tracker colocalization experiment

Stock solution of trackers for mitochondria, lysosome and ER were diluted with cell culture medium into 100 nM, 500 nM and 4 μM respectively. RB-EPP 6 was added into each

working solution at 500 nM. U87 cells were incubated with the both trackers and RB-EPP 6 for 1 h and then washed once before confocal imaging.

Heparin binding assay

U87 cells were treated with Heparin sulfate at 10, 20, 50, 100, 200 μg/ml in 5% CO_2 incubator at 37 °C for 30 min. Afterwards, cell medium was replaced by medium with both heparin sulfate and 500 nM RB-EPP6 for another 1 h incubation. A trypsin-EDTA solution (0.05%, Sigma) was added to detach the cells. The cells were collected by centrifugation. Fresh phenol-free medium was added to each condition. Once resuspended, cells were filtered into glass tubes before flow cytometry.

Octanol-water partition assay

For each RB-EPP, pre-mix 250 μl of octanol with 250 μl of water in a 1.5 ml centrifuge tube. 2 μl of RB-EPP was added to the solution at the concentration of 500 μM. After vortex the mixture, centrifuge at the highest speed for 10 min to separate the octanol and water phases. Samples were collected from both phases and quantified by the Analytical HPLC separately.

RNA-seq studies

In a 100x15 mm dish, 1m U87 cells were seeded for overnight culture in full DMEM medium containing 10% FBS and 1% PS. RB-EPP 6 diluted with fresh culture medium at 500 nM was used to replace the old medium the next day. After 1 h incubation in the 5%

CO_2 incubator at 37 °C, the cells were treated with trypsin and resuspended in fresh phenol-free medium after centrifuge. Then, cells were filtered into glass tubes for fluorescence-activated cell sorting (FACS). Cells with the highest and lowest 30% fluorescence intensity was collected separately. RNA extraction was performed using the RNeasy Micro Kit (50) right after FACS experiment.

FIBCD1 competition assay

U87 cells were incubated with 500 nM RB-EPP 6 and YOYO, together with FIBCD1 ligands, sodium acetate (SA) at 3.1 mM (1x) and acetylmannosamine (AMA) at 1.6 mM (1x) respectively. After 1 h, trypsin was added to detach the cells. Cell pallets were collected by centrifugation. Fresh phenol-free medium was added to each condition. Once resuspended, cells were filtered into glass tubes before flow cytometry.

Plasmid transfection assays

300 k U87 cells were seeded in the 35x10 mm dish for overnight culture. Plasmids (caveolin, 75 ng; clathrin, 100 ng; rab5, 100 ng; rab7a, 100ng; caveolin-1 CRISPR/Cas9 KO, 3 μg; FIBCD1 CRISPR/Cas9 KO, 3 ug; Control CRISPR, 3 ug) were diluted with Plasmid Transfection Medium (sc-108062) to 50 μl. UltraCruz Transfection Reagent (Santa Cruz Biotechnology) was also diluted with Plasmid Transfection Medium to 50 μl. Plasmids and transfection reagent were mixed well and kept at room temperature for 20 min. Replace the cells with PS free medium and add the mixture to the cells, culture for another 24 h.

MDCK transwell assay

200 k MDCK cells were seeded in 200 µl in complete growth media to the apical side of a transwell insert (12-well 8 µm pore size Transwell-65 mm). In addition, 1 ml complete growth media is added to the basolateral chamber. Six transwell inserts were prepared for a randomized peptide labeled with RB (RB-GSQTH), and six other inserts are prepared for RB-EPP 6. Incubate the plate for 2-3 days at 37 °C with 5% CO_2. The electrical resistance of MDCK transwell inserts was measured using EVOM Epithelial Voltohmmeter to measure the integrity of tight junctions the following two days. On day 3, serum free media was used to wash both the apical (200 µl) and basolateral (1 ml) wells three times. Cells were kept in a 37 °C/5% CO_2 cell incubator equilibrating for 15 min.

The assay was carried out in both apical to basolateral and basolateral to apical direction. Both RB-GSQTH and RB-EPP 6 were prepared at 10 µM in serum free media. For the assay with apical to basolateral direction, the apical chamber was replaced with 200 µl testing compounds. For the assay with basolateral to apical direction, the basolateral chamber was replaced with 1 ml testing compounds. Both plates were incubated in the cell culture incubator for 3 h. After that, 80 µl of the samples were collected from each chamber for RB fluorescence intensity reading using a Synergy H1 microplate reader.

PAMPA assay

All the RB-EPPs were diluted in PBS to 100 µM. 700 µl of the testing peptides were added to the apical chamber of a Corning BioCoat Pre-coated PAMPA Plate. 200 µl PBS was

added to the basolateral chamber. The plate was kept at 37 °C with 5% CO_2 for 5 h. After that, 80 µl samples were collected from each chamber for RB fluorescence intensity reading using the Synergy H1 microplate reader.

Lipid binding assay

95% egg PC, 5% nitrobenzoxadiazole (NBD) were added to 1% cholesterol, PE, PG, ganglioside, SM and PA to make liposomes individually. RB-EPP 6 was diluted with HEPES buffer to different concentrations, ranging from 1 nM to 10 µM. For each lipid type, 400 µl liposomes of 50 µg/ml were added to 400 µl of each RB-EPP 6 concentration. The mixture was incubated at room temperature for 15 min. 80 µl of each condition was collected to measure the fluorescence intensity of NBD suing the Synergy H1 microplate reader.

Ethidium bromide (EB) staining

U87 cells were incubated with 2 µg/ml EB with or without the conjugation of EPP6 for an hour, 3 hours and 6 hours respectively. After 1 h and the cells were washed with fresh phenol-free media once before confocal imaging.

Statistical analysis

Pearson's correlation coefficient was used to calculate correlation between RB and tracker channels in the organelle tracker experiment. Graph generation and statistical analyses were performed using Fiji software.

4.3 Results and Discussion

Hydoxyl-rich cyclic peptides bring cargo molecules into cells

We prepared seven hydroxyl-rich cyclic peptides using tyrosine, threonine, and serine as the building blocks. These peptides had five modular amino acid positions and were cyclized through a triazole ring (Fig. 4.1a, b), and the exposed N terminal allowed for cargo conjugation. In our first example, we linked EPPs to a Rhodamine B (RB) tag and assessed their abilities to enter the cells. We chose U87 cell line as the model system and used confocal imaging to evaluate the intracellular fluorescence (Fig. 4.1c). As shown in Fig. 4.1d, these EPPs had differential abilities to enter the cells, with EPP6 demonstrating the highest efficiency. Compared with the benchmark, TAT peptide, EPP6 led to ~2X fluorescence intensity in the cells. More interestingly, we found that increasing EPP6 concentration led to higher fluorescence signals across a wide range (Fig. 4.2). In our subsequent studies, we focus on EPP6 as the model compound.

Considering that the size of EPP6 and the RB tag was comparable, and RB was known to interact with the cell membrane, we must confirm that EPP6, rather than the RB tag, was the critical component that led to the uptake. Therefore, we conjugated EPP6 to different fluorescent dye molecules and performed similar uptake experiments using U87 cells. Our results proved that EPP6 could bring all these cargo molecules into U87 cells (Fig. 4.3a). It is worth pointing out that AF555 and AF647 are negatively charged dyes and exhibit negligible interaction with the cell membrane. Therefore, our results confirmed that it was the EPP6 moiety that enabled the uptake.

We then sought to test if the observed EPP6 uptake was limited to U87 cells. We incubated RB-EPP6 with different cell lines and evaluated the intracellular fluorescence intensities. As shown in Fig. 4.3b, EPP6 was able to enter a wide array of human cancer and noncancer cells, as well as non-human cells. Nevertheless, the resulting intracellular fluorescence intensities varied significantly across different cell lines, which prompted us to further investigate the mechanism of cell entry.

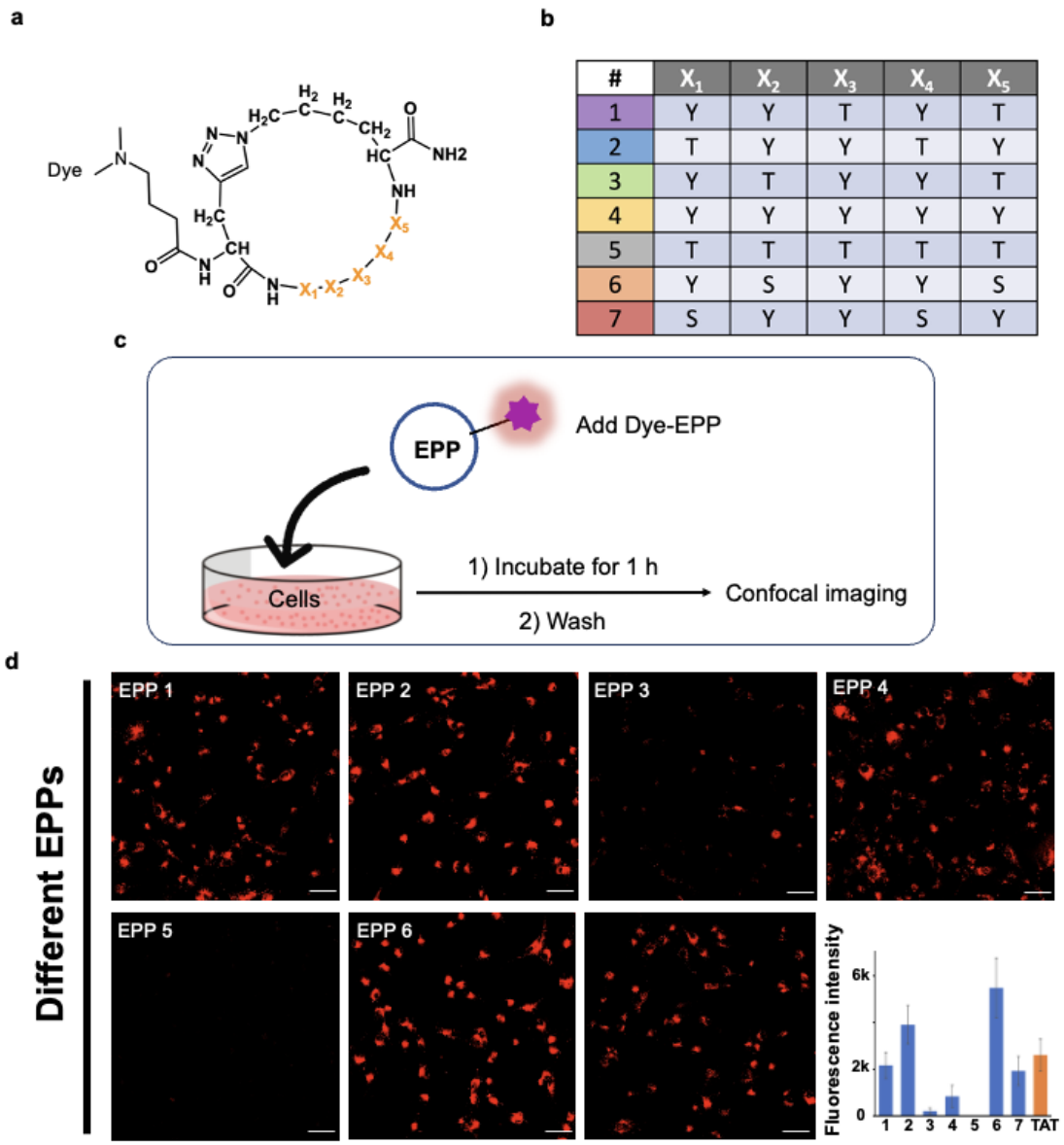

#	X_1	X_2	X_3	X_4	X_5
1	Y	Y	T	Y	T
2	T	Y	Y	T	Y
3	Y	T	Y	Y	T
4	Y	Y	Y	Y	Y
5	T	T	T	T	T
6	Y	S	Y	Y	S
7	S	Y	Y	S	Y

Fig. 4.1 Hydroxyl-rich cyclic peptides facilitate the transportation of cargo molecules into cells. (**a**) Generic structure of the EPPs. (**b**) Sequences of EPP1-7. (**c**) General method for assessing EPP uptake. (**d**) Confocal images showing that EPPs were able to bring rhodamine B (RB) tag into U87 cells with different efficiencies. The scale bar shows 50 μm. The bar graph shows the single-cell intracellular fluorescence intensities quantified from the confocal images. The error bars denote the standard deviation. RB-TAT was used for comparison.

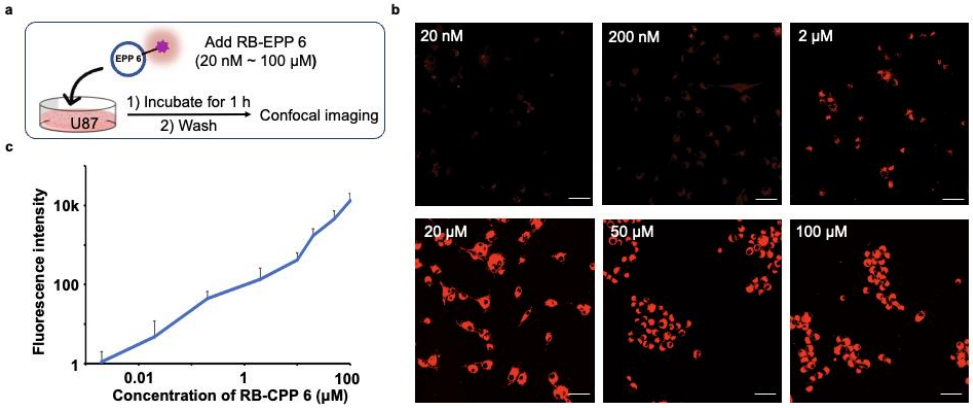

Fig. 4.2 Concentration-dependent uptake of RB-EPP6. (**a**) Illustration of the incubation process of RB-EPP6 at different concentrations in U87 cells. (**b**) Confocal images showing the uptake of RB-EPP6 by U87 cells increased as the concentration of RB-EPP6 gets higher. (**c**) The line chart shows the single-cell intracellular fluorescence intensities quantified from the confocal images.

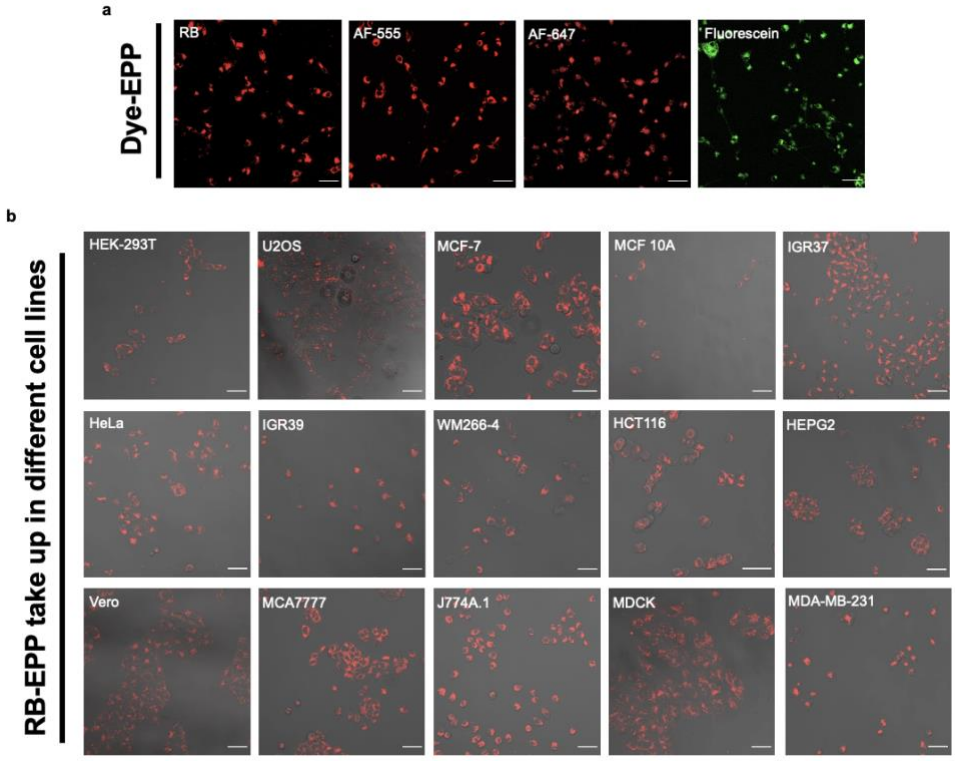

Figure 4.3 (**a**) Confocal images showing that EPP6 was able to bring different cargo molecules into the cells. The scale bar shows 50 μm. (**b**) Confocal images showing that RB-EPP6 was taken up by a wide panel of cell lines. The scale bar shows 50 μm.

EPP6 enters the cells through caveolin- and dynamin-dependent endocytosis

Unlike the well-studied positively charged CPPs (TAT, penetrating, poly-R, CPP12, etc.), these EPPs did not have charged residues. On the other hand, the hydroxyl groups may form intramolecular hydrogen bonds that render the EPPs hydrophobic. Because hydrophobic peptides are known to penetrate the cell membrane autonomously, it was possible that the EPPs entered the cells due to hydrophobicity. To test this hypothesis, we performed the octanol partitioning experiment to assess the hydrophobicity of RB-EPPs (Fig. 4.4a). Interestingly, most of the RB-EPPs were not strongly hydrophobic (Fig. 4.4b). Particularly, the best performing candidate, RB-EPP6, appeared to be hydrophilic, while the worst one, RB-EPP3, was the most hydrophobic. These results proved that hydrophobicity was not the driving force of EPP function.

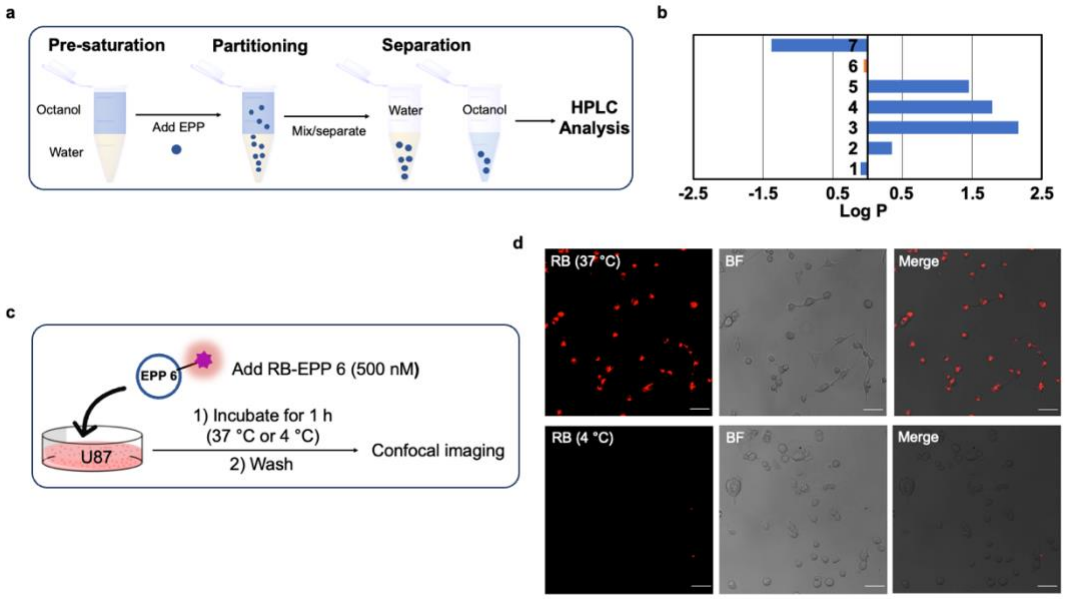

Fig. 4.4 EPP6 entered the cell through an energy-dependent process. (**a**) Illustration of the octanol partitioning experiment. (**b**) Results of the octanol partitioning experiments. Most of the EPPs showed a positive logP value. (**c**) Illustration of the process for comparing RB-EPP6 uptake at different temperatures. (**d**) Confocal images showing that low-temperature incubate led to no RB-EPP6 uptake in U87 cells. The scale bar shows 50 μm.

We then tested whether EPPs entered the cells through passive diffusion or active transportation. We incubated U87 cells with RB-EPP6 at 37 °C and 4 °C, and subsequently used confocal imaging to assess the intracellular fluorescence intensities (Fig. 4.4c). As shown in Fig. 4.4d, the low-temperature treatment led to no fluorescence signal in the cells, suggesting that RB-EPP6 entered the cells through an energy-dependent process. To validate our findings, we further performed the parallel artificial membrane permeability assay (PAMPA) to evaluate the passive diffusion abilities of the EPPs (Fig. 4.5). We found that EPPs could not pass through the artificial membrane, which further supported our conclusion that EPPs entered the cells through active transportation mechanisms.

a

	Pe (cm/s)	logPe
EPP 3	1.1206E-07	-7.0
EPP 1	1.6201E-07	-6.8
EPP 6	2.34E-07	-6.6
EPP 2	4.6872E-07	-6.3
EPP 7	6.3243E-07	-6.2
TAT	1.2276E-06	-5.9
EPP 5	1.8954E-06	-5.7

b

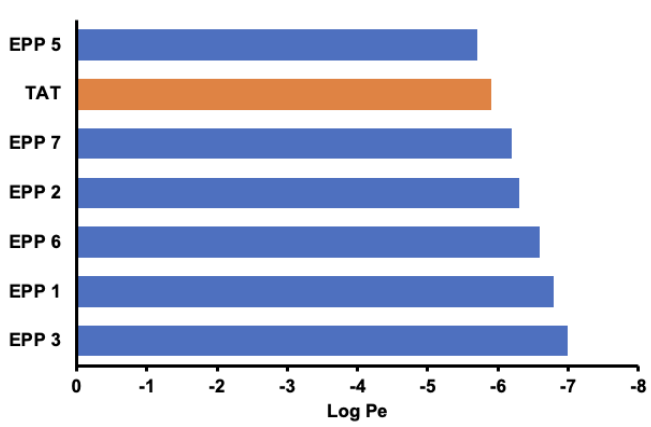

Fig. 4.5 (**a**) PAMPA assay results of EPPs. (**b**) The bar graph shows PAMPA value for each EPP quantified from the table on the left.

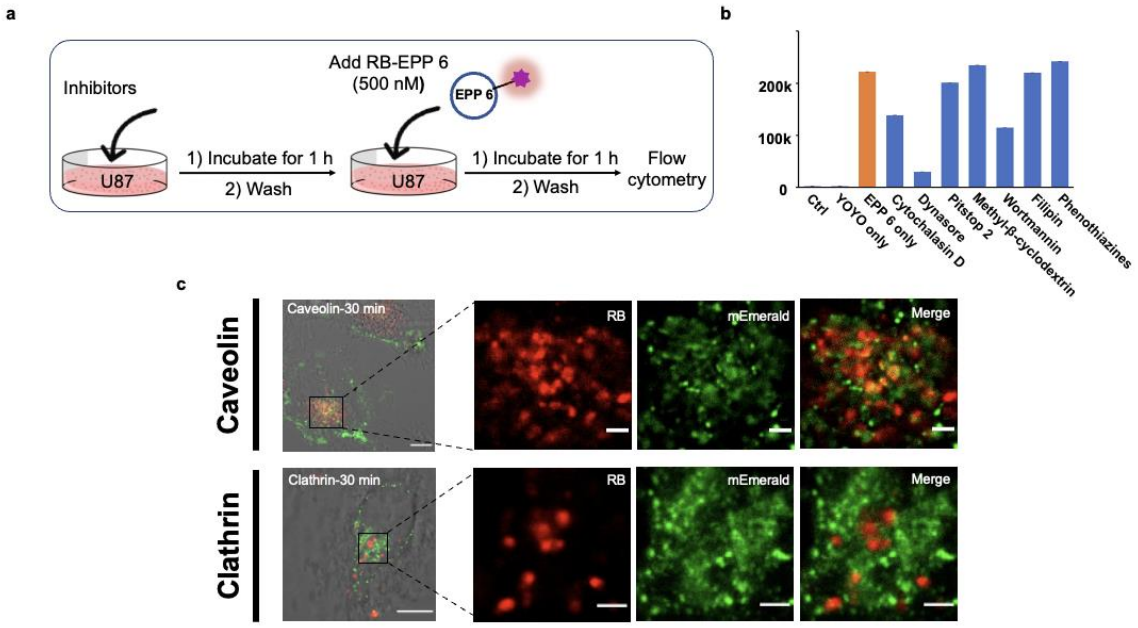

Fig. 4.6 EPP6 enters the cells through a dynamin- and caveolin-dependent endocytosis pathway. (**a**) Illustration of the endocytosis inhibitor tests. (**b**) Flow cytometry results showing the effects of inhibitors on the uptake of RB-EPP6 in U87 cells. (**c**) Representative confocal images showing the overlap between mEmerald-caveolin and RB-EPP6. No significant colocalization was observed between mEmerald-clathrin and RB-EPP6. The scale bar shows 10 μm.

Considering the size of the EPPs, and that different dye conjugates were all able to enter the cells, we reasoned that the transportation was unlikely to involve transmembrane transporter proteins or ion channels. Therefore, an endocytosis pathway was the more plausible mechanism. To identify the critical components in EPP transportation, we used a panel of inhibitors targeting various parts of common endocytosis pathways. We incubated U87 cells with RB-EPP6 in the presence of these inhibitors and used flow cytometry to compare the resulted fluorescence intensities (Fig. 4.6a). As shown in Fig. 4.6b, dynamin inhibition (Dynasore) almost completely suppressed RB-EPP6 uptake, which suggested a dynamin-dependent endocytosis pathway. Similarly, inhibition of actin polymerization

(cytochalasin D) and PI3K signaling (wortmannin) caused significantly decreased RB-EPP6 uptake, albeit not as prominent as that from the dynamin inhibition. In contrast, inhibitors of clathrin-mediated endocytosis (Pitstop 2 and phenothazine) did not affect the uptake, which pointed to a clathrin-independent process. Based on the current picture of endocytosis pathways, these results hinted at a caveolin-mediated endocytosis pathway.

To further delineate the roles of caveolin and clathrin, we transfected U87 cells with mEmerald-caveolin and mEmerald-clathrin plasmids, incubated the cells with RB-EPP6, and assessed the resulted intracellular fluorescence. We observed that the RB-EPP6 signal significantly overlapped with the mEmerald-caveolin fluorescence, while no overlap existed between RB-EPP6 and mEmerald-clathrin (Fig. 4.6c). This result further validated our hypothesis that EPP6 enters the cells through the caveolin-dependent pathway.

Interestingly, we further found that cholesterol extraction (methyl-β-cyclodextrin) and cholesterol binding (filipin) did not inhibit RB-EPP6 uptake (Fig. 4.6b). These results were unusual because most caveolin-mediated endocytosis mechanisms involve cholesterol and lipid rafts. To validate our finding, we tested the binding affinity between RB-EPP6 and cell membrane lipid components. Our results confirmed that there was no appreciable interaction between RB-EPP6 and lipids (Fig. 4.7). Another popular pathway of caveolin-dependent endocytosis relies on heparan sulfate proteoglycans (HSPG), which is implicated in the uptake of some well-established CPPs and many other macromolecules. However, high concentrations of heparin did not affect RB-EPP6 uptake (Fig. 4.8), which suggested that HSPG was not involved. Taken together, our results suggested that EPP6

took an uncommon mechanism within the premises of dynamin- and caveolin-dependent endocytosis pathway, perhaps through a receptor-mediated endocytosis process.

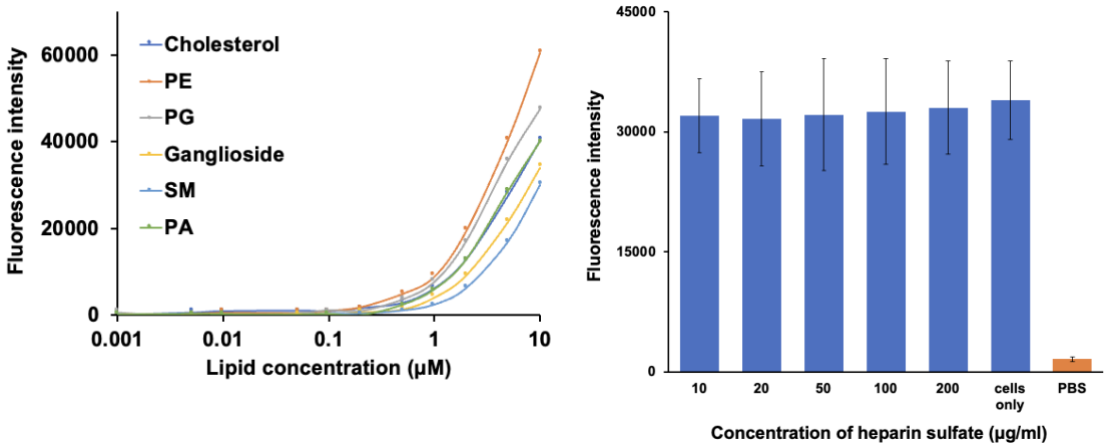

Fig. 4.7 (left). Lipid binding assay results indicating no significant interaction between lipid components and RB-EPP6.

Fig. 4.8 (right). Heparin binding assay. The bar graph shows that heparin exhibited no inhibitory effect towards RB-EPP6 uptake in U87 cells quantified from flow cytometry.

FIBCD1 is a surface receptor for EPP6 recognition

To better understand the EPP6 endocytosis mechanism, we resorted to identifying the genes involved in the uptake. We incubated U87 cells with RB-EPP6 and used a fluorescence-activated cell sorter to isolate the top 30% and the bottom 30% populations based on the RB-channel cellular fluorescence. We extracted RNAs from these two populations as well as the control (untreated) cells and carried out transcriptome analysis by RNA-seq (Fig. 4.9a). We prepared three biological repeats for each condition, and generated on average 30 million reads per sample. The raw data was processed using fastp, STAR, and featureCounts to generate annotated gene lists, and the differentially expressed genes between the samples were identified by DESeq2. Here, we aimed to find upregulated genes in the high-uptake samples that could be receptors for EPP6 uptake. We first

compared the high-uptake samples with the low-uptake ones. Based on the criteria of $p < 0.0001$ and > 2-fold changes, we found one gene, fibrinogen C domain-containing protein 1 (FIBCD1), stood out during the process and we hypothesized that it was the receptor responsible for EPP6 uptake (Fig. 4.9b).

FIBCD1 is a type II transmembrane receptor, and it is known to induce endocytosis. Its natural ligands are mono- and oligosaccharides, including acetylmannosamine, chitin, β-1,3-glucan, and galactomannan. Notably, significant structural similarities exist between these ligands and the EPPs, as they all present abundant hydroxyl groups. Such similarities supported our hypothesis that FIBCD1 was the receptor for EPP6 uptake. To further validate our hypothesis, we performed a competition experiment where U87 cells were incubated with RB-EPP6 with and without acetylmannosamine – a potent FIBCD1 ligand (Fig. 4.9c). Our results showed that acetylmannosamine was able to inhibit RB-EPP6 uptake in a concentration-dependent manner (Fig. 4.9d).

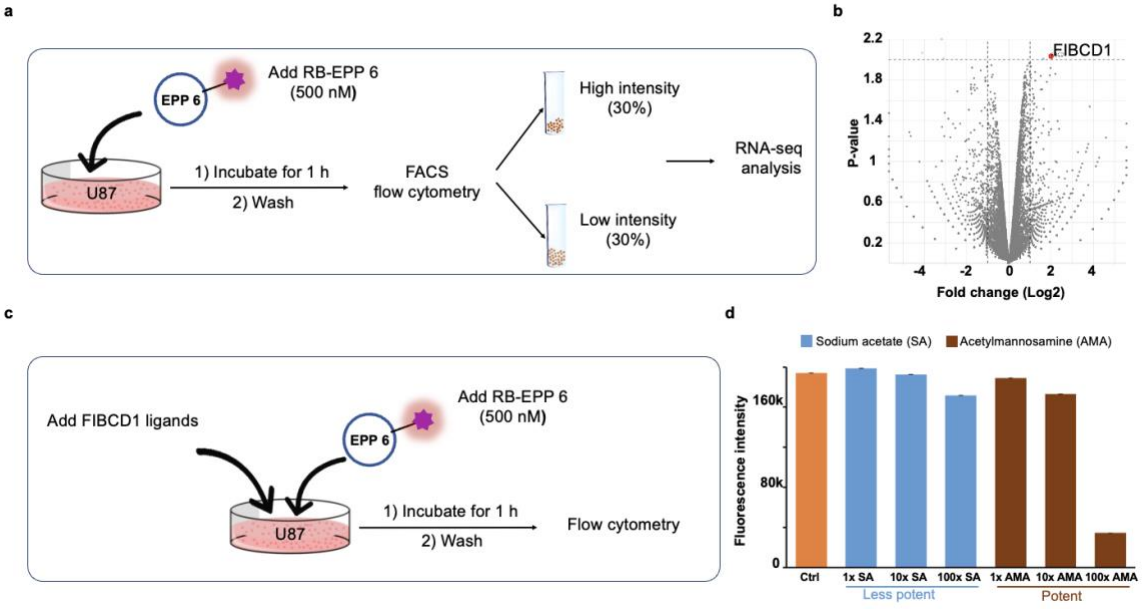

Fig. 4.9 FIBCD1 is a surface receptor for EPP6 recognition. (**a**) Illustration of the sample preparation for RNA-seq. (**b**) RNA-seq results identifying the FIBCD1 gene as the potential receptor for EPP6. The red dot in the graph represents the FIBCD1 gene. (**c**) Illustration of the process for comparing RB-EPP6 uptake at the presence of different FIBCD1 ligands. (**d**) Flow cytometry results showing the effects of FIBCD1 ligands on the uptake of RB-EPP6 in U87 cells.

Intracellular fate of EPP6

We sought to investigate the fate of EPP6 after endocytosis. Typical cargo molecules go through the early endosome – late endosome – lysosome pathway after endocytosis, while many well-established CPPs could escape from the endosomes and achieve cytosolic delivery. We hypothesized that EPP6 would adopt a similar pathway. To label the endosomes, we transfected U87 cells with EGFP-Rab5 (early endosome marker) and mEmerald-Rab7a (late endosome marker). We incubated these cells with RB-EPP6 and used confocal microscopy to analyze the colocalization of RB-EPP6 with the fluorescent markers. As shown in Fig. 4.10a, after 15-min, RB-EPP6 appeared in distinct Rab5-coated vesicles, indicating that RB-EPP6 traveled into early endosomes quickly after the

endocytosis. Meanwhile, no obvious colocalization was observed between Rab7a-labeled vesicles and RB-EPP6. At 30 minutes, RB-EPP6 disappeared from the Rab5-labeled vesicles and appeared in Rab7a-labeled vesicles. This transition suggested that RB-EPP6 trafficked into late endosomes within 30 minutes. Interestingly, we found that a significant amount of RB-EPP6 remained inside Rab7a+ vesicles even after 4 hours.

To further investigate the intracellular trafficking of RB-EPP6 after endocytosis, we used LysoTracker to label the lysosomes and assessed the signal colocalization. We found that some RB-EPP6 signals appeared in lysosomes after 3 hours (Fig. 4.10b). Nevertheless, many RB-EPP6-containing vesicles were not in lysosomes even after 6 hours, which was consistent with our results that the RB-EPP6 signal remained in Rab7a+ vesicles. It is worth pointing out that in addition to the obvious punctuated RB-EPP6 signal, there was also significant smearing of the signals that indicated cytosolic distribution. Indeed, such smeared signals were obvious at 1 hour and became more prominent after 3 hours (Fig. 4.10c). Interestingly, some signals remained even after 24 hours. More importantly, a significant amount of the remaining signal was punctuated. Because endosomes and lysosomes do not have a long lifetime, these punctate signals suggested that RB-EPP6 remained in other long-live vesicles. In addition, we also validated that RB-EPP6 did not traffic into the mitochondria or the endoplasmic reticulum (Fig. 4.10d).

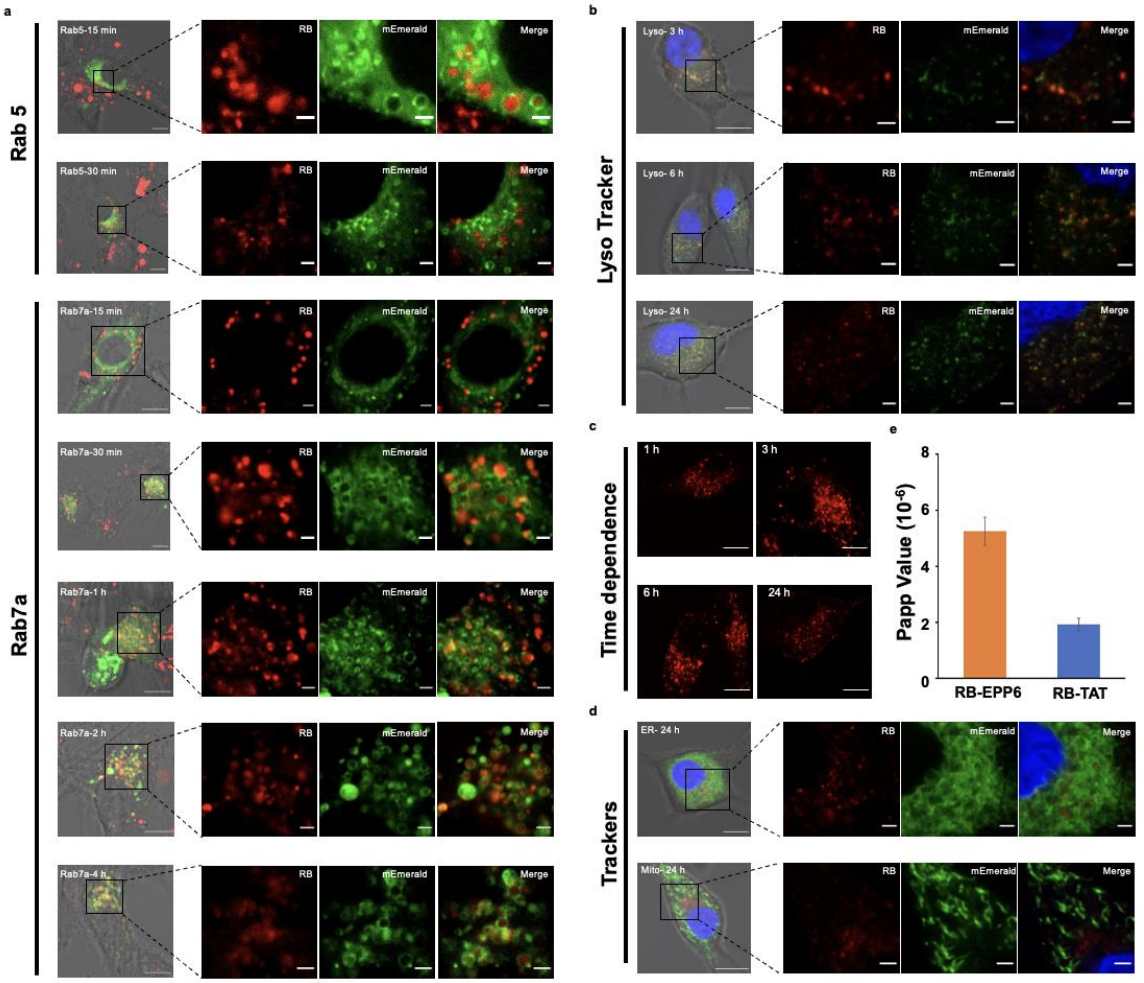

Fig. 4.10 Intracellular fate of EPP6. (**a**) Representative confocal images showing the overlap between EGFP-Rab5 and RB-EPP6 at 15 min. Significant colocalization was observed between mEmerald-Rab7a and RB-EPP6 starting at 30 min, the colocalization lasted for up to 4 hours. (**b**) Representative confocal images showing overlaps between LysoTracker and RB-EPP6. The scale bar shows 10 μm in the original images on the left and 2 μm in the zoomed in images on the right. (**c**) Representative confocal images showing RB-EPP6 signals in U87 cells at a time-dependence manner. The scale bar shows 10 μm. (**d**) Representative confocal images showing overlaps between different trackers and RB-EPP6, ERTracker (upper) and MitoTracker (lower). The scale bar shows 10 μm in the original images on the left and 2 μm in the zoomed in images on the right. (**e**) The bar graph showing the Papp values for RB-EPP6 and RB-TAT.

Considering that the intracellular signal decreased over time, we hypothesized that a part of the cargo molecules might exit the cells through exocytosis, which might further enable transcytosis. To test this hypothesis, we prepared tight cell monolayers in a trans-well apparatus using MDCK cells, and assessed the apical transcytosis rate of RB-EPP6. We also included RB-TAT for comparison. After three hours of incubation, we quantified the target molecule concentrations in the apical and basal chambers, and calculated the Papp values. We found that RB-EPP6 exhibited a Papp value of 5.25×10^{-6}, which was about three times that of RB-TAT (Fig. 4.10e).

4.4 Conclusion

Molecularly defined delivery tags can bring cargo molecules into cells through endocytosis, and they have profound research and therapeutic applications. Because their sizes are often comparable to, if not smaller than, the cargo, the delivery efficiency is cargo-dependent. Consequently, there are no universally effective delivery tags for all cargos, and there remains a pressing need to expand the collection. The endocytosis-promoting peptides (EPPs) presented here represent a new category of delivery tags. They are hydrophilic and uncharged, and they are able to transport a wide array of small-molecule cargos into a diverse panel of animal cells.

The lack of charge is the key feature that differentiates EPPs from conventional CPPs. All existing hydrophilic CPPs are positive charged, which is deemed necessary for the initial steps of endocytosis. Nevertheless, the premise of this notion is that positively charged CPPs interact with negatively charged membrane components such as lipids and HSPGs, which is only a fraction of the mechanisms that can trigger endocytosis. Therefore, it is

natural to hypothesize that peptide sequences without positive charges may also trigger endocytosis, perhaps through the receptor-mediated pathways. Indeed, our EPP results support this hypothesis and prove that positive charge is not an indispensable part of peptide-based delivery tags.

In our study, we found that EPP6 entered cells through FIBCD1-mediated endocytosis that was dependent on caveolin and dynamin. FIBCD1 is implicated in pathogen recognition, where it binds to specific saccharides. It is known to induce endocytosis, but the detailed mechanism remains elusive. Our results indicate that FIBCD1-mediated endocytosis required actin, dynamin, and caveolin, which provided a clearer picture of the endocytic process of FIBCD1. On the other hand, our findings also underscore the complexity of endocytosis pathways, especially the caveolin-dependent endocytosis. Existing studies highlight the critical role of lipid rafts in caveolin-dependent endocytosis, as the membrane enrichment of caveolin relies on these cholesterol-rich regions. However, we found that cholesterol-binding agents (filipin and methyl-cyclodextrin) did not affect RB-EPP6 uptake, proving that caveolin-dependent endocytosis can also take a lipid raft-independent route. In addition, our results echo the emerging opinion that the specificity of inhibitors shall be carefully considered when studying the endocytosis pathway.

Our results have delineated the intracellular fate of EPP, but a few connecting pieces remain missing from the picture. The imaging results of RB-EPP6 and EB-EPP6 proved that a significant amount of EPP6 could escape from the endosomes and enter the cytosol, but the molecular mechanism of this process was unclear. Because EPP6 is not charged or hydrophobic, common CPP escape mechanisms such as osmotic rupture and budding are

not applicable here. Similarly, the punctate signals after 24 hours suggest that some RB-EPP6 trafficked to long-lived vesicles. The identity of these vesicles and the underlying mechanism of this trafficking call for future studies.

The presented EPPs have immediate therapeutic implications. Since EPP6 could bring strongly negatively charged molecules (AF555 and AF647) into the cell, exploring its application in DNA/RNA delivery is intriguing. On the other hand, because the expression of caveolin and FIBCD1 varies significantly across different tissues and organs, it is also possible to leverage this difference and tailor the EPP delivery for specific targets. For instance, the high expression levels of FIBCD1 and caveolin in the digestive tract may allow efficient gastrointestinal drug delivery and absorption. In addition, the Papp value of RB-EPP6 (5.3×10^{-6}) is higher than the cutoff threshold of CNS availability (3.5×10^{-6}), which hints at its potential of crossing the blood-brain barrier. Finally, our discovery of the EPPs encourages us to discover more tags targeting different endocytic receptors, further diversifying the arsenal of delivery tags for research and therapeutic applications.

4.5 References

1. Macara, I. G., Transport into and out of the nucleus. *Microbiology and molecular biology reviews* **2001,** *65* (4), 570-594.

2. Ross, J. L.; Ali, M. Y.; Warshaw, D. M., Cargo transport: molecular motors navigate a complex cytoskeleton. *Current opinion in cell biology* **2008,** *20* (1), 41-47.

3. Mukherjee, S.; Ghosh, R. N.; Maxfield, F. R., Endocytosis. *Physiological reviews* **1997**.

4. Besterman, J. M.; Low, R. B., Endocytosis: a review of mechanisms and plasma membrane dynamics. *Biochemical Journal* **1983,** *210* (1), 1-13.

5. Mettlen, M.; Chen, P.-H.; Srinivasan, S.; Danuser, G.; Schmid, S. L., Regulation of clathrin-mediated endocytosis. *Annual review of biochemistry* **2018,** *87*, 871-896.

6. Madsen, S. J.; Hirschberg, H., Macrophages as delivery vehicles for anticancer agents. *Therapeutic delivery* **2019,** *10* (3), 189-201.

7. Bazzani, L.; Donnini, S.; Giachetti, A.; Christofori, G.; Ziche, M., PGE2 mediates EGFR internalization and nuclear translocation via caveolin endocytosis promoting its transcriptional activity and proliferation in human NSCLC cells. *Oncotarget* **2018,** *9* (19), 14939.

8. Peer, D.; Karp, J. M.; Hong, S.; Farokhzad, O. C.; Margalit, R.; Langer, R., Nanocarriers as an emerging platform for cancer therapy. *Nature nanotechnology* **2007,** *2* (12), 751-760.

9. Pattni, B. S.; Chupin, V. V.; Torchilin, V. P., New developments in liposomal drug delivery. *Chemical reviews* **2015,** *115* (19), 10938-10966.

10. Anselmo, A. C.; Mitragotri, S., Nanoparticles in the clinic. *Bioengineering & translational medicine* **2016,** *1* (1), 10-29.

11. Silva, S.; Almeida, A. J.; Vale, N., Combination of cell-penetrating peptides with nanoparticles for therapeutic application: a review. *Biomolecules* **2019,** *9* (1), 22.

12. Gessner, I.; Neundorf, I., Nanoparticles modified with cell-penetrating peptides: Conjugation mechanisms, physicochemical properties, and application in cancer diagnosis and therapy. *International journal of molecular sciences* **2020,** *21* (7), 2536.

13. Zhao, R.; Diop-Bove, N.; Visentin, M.; Goldman, I. D., Mechanisms of membrane transport of folates into cells and across epithelia. *Annual review of nutrition* **2011,** *31*, 177-201.

14. Sharma, G.; Lakkadwala, S.; Modgil, A.; Singh, J., The role of cell-penetrating peptide and transferrin on enhanced delivery of drug to brain. *International journal of molecular sciences* **2016,** *17* (6), 806.

15. Smith, B. A.; Daniels, D. S.; Coplin, A. E.; Jordan, G. E.; McGregor, L. M.; Schepartz, A., Minimally cationic cell-permeable miniature proteins via α-helical arginine display. *Journal of the American Chemical Society* **2008,** *130* (10), 2948-2949.

16. Snyder, E. L.; Dowdy, S. F., Cell penetrating peptides in drug delivery. *Pharmaceutical research* **2004,** *21* (3), 389-393.

17. Derakhshankhah, H.; Jafari, S., Cell penetrating peptides: A concise review with emphasis on biomedical applications. *Biomedicine & Pharmacotherapy* **2018,** *108*, 1090-1096.

18. Ramsey, J. D.; Flynn, N. H., Cell-penetrating peptides transport therapeutics into cells. *Pharmacology & therapeutics* **2015,** *154*, 78-86.

19. Zou, L.; Peng, Q.; Wang, P.; Zhou, B., Progress in research and application of HIV-1 TAT-derived cell-penetrating peptide. *Journal of Membrane Biology* **2017,** *250* (2), 115.

20. Mokhtarieh, A. A.; Kim, S.; Lee, Y.; Chung, B. H.; Lee, M. K., Novel cell penetrating peptides with multiple motifs composed of RGD and its analogs. *Biochemical and biophysical research communications* **2013,** *432* (2), 359-364.

21. Letoha, T.; Gaál, S.; Somlai, C.; Czajlik, A.; Perczel, A.; Penke, B., Membrane translocation of penetratin and its derivatives in different cell lines. *Journal of Molecular Recognition* **2003,** *16* (5), 272-279.

22. Hu, C.; Chen, X.; Huang, Y.; Chen, Y., Co-administration of iRGD with peptide HPRP-A1 to improve anticancer activity and membrane penetrability. *Scientific reports* **2018,** *8* (1), 1-14.

23. Song, J.; Qian, Z.; Sahni, A.; Chen, K.; Pei, D., Cyclic cell-penetrating peptides with single hydrophobic groups. *Chembiochem: a European journal of chemical biology* **2019,** *20* (16), 2085.

24. Habault, J.; Poyet, J.-L., Recent advances in cell penetrating peptide-based anticancer therapies. *Molecules* **2019,** *24* (5), 927.

25. Kang, Z.; Ding, G.; Meng, Z.; Meng, Q., The rational design of cell-penetrating peptides for application in delivery systems. *Peptides* **2019,** *121*, 170149.

26. Kurrikoff, K.; Langel, Ü., Recent CPP-based applications in medicine. *Expert opinion on drug delivery* **2019,** *16* (11), 1183-1191.

27. Ye, J.; Liu, E.; Yu, Z.; Pei, X.; Chen, S.; Zhang, P.; Shin, M.-C.; Gong, J.; He, H.; Yang, V. C., CPP-assisted intracellular drug delivery, what is next? *International journal of molecular sciences* **2016,** *17* (11), 1892.

28. Ding, Y.; Cui, W.; Sun, D.; Wang, G.-L.; Hei, Y.; Meng, S.; Chen, J.-H.; Xie, Y.; Wang, Z.-Q., In vivo study of doxorubicin-loaded cell-penetrating peptide-modified pH-sensitive liposomes: biocompatibility, bio-distribution, and pharmacodynamics in BALB/c nude mice bearing human breast tumors. *Drug design, development and therapy* **2017,** *11*, 3105.

29. Jones, S. W.; Christison, R.; Bundell, K.; Voyce, C. J.; Brockbank, S. M.; Newham, P.; Lindsay, M. A., Characterisation of cell-penetrating peptide-mediated peptide delivery. *British journal of pharmacology* **2005,** *145* (8), 1093-1102.

30. Qian, Z.; Martyna, A.; Hard, R. L.; Wang, J.; Appiah-Kubi, G.; Coss, C.; Phelps, M. A.; Rossman, J. S.; Pei, D., Discovery and mechanism of highly efficient cyclic cell-penetrating peptides. *Biochemistry* **2016,** *55* (18), 2601-2612.

31. Kalafatovic, D.; Giralt, E., Cell-penetrating peptides: Design strategies beyond primary structure and amphipathicity. *Molecules* **2017,** *22* (11), 1929.

32. Ruseska, I.; Zimmer, A., Internalization mechanisms of cell-penetrating peptides. *Beilstein journal of nanotechnology* **2020,** *11* (1), 101-123.

33. Xu, P.; Van Kirk, E. A.; Zhan, Y.; Murdoch, W. J.; Radosz, M.; Shen, Y., Targeted charge-reversal nanoparticles for nuclear drug delivery. *Angewandte Chemie International Edition* **2007,** *46* (26), 4999-5002.

Chapter 5: Conclusion remarks

In this thesis, we have demonstrated three studies toward the biochemical applications of monocyclic peptides. In chapter 2, we have synthesized a monocyclic peptide library and screened it against lipid A at its native form. From the screening, we found a peptide with inhibitory effects towards LPS toxicity. Our study has showcased the feasibility of identifying monocyclic peptide hits against a complex target such as LPS, whose structure is not well-defined. Besides, our study also underscored the possibility of neutralizing lipid A toxicity using a novel LPS-neutralization compound with much lower toxicity comparing to the current solutions. Other than that, since the LPS inhibitory effect of our peptides appeared to be limited, more screening efforts using other libraries should be explored in future research. For example, more complex libraries composed of bicyclic peptides can be employed for screening. Besides that, we can also try to expand the LPS strains to study the efficacy for the hit ligands in the future.

In chapter 3, we have established a method using digitonin as a generalized delivery tool to target cell membranes specifically. Using this strategy, we also successfully transferred monocyclic peptides into a wide range of suspension cells, including the adherent cell suspension, lymphoid and myeloid cells. Moreover, we demonstrates the analysis of AKT signaling activities in different cell lines under drug perturbations. Overall, the study of single-cell kinase signaling dynamics is important because it can help identify cell subpopulations and guide therapeutic decisions. Our study has showcased an analytical workflow that enables the analysis of the kinase signaling dynamics for clinical samples in the single-cell suspension format. Our work has provided insight into the study of protein

signaling activities, which can help us further optimize therapeutic solutions in this field. Other than that, we did realize the limitation of our study. We may need to test different concentrations for each cell type in terms of digitonin usage, which might be labor-intense but meanwhile it encouraged us to study or improve other molecular transfer techniques in the future.

In chapter 4, We have designed a group of novel cell-penetrating peptides that are hydrophilic and uncharged. We demonstrated that EPP6, the one that has the highest uptake efficiency among the peptides, can transport a wide array of small-molecule cargos into a diverse panel of animal cells.

Most importantly, our study showed that the interactions between the cell membrane and uncharged peptides could be facilitated through receptor-mediated pathways.

It has been recognized that there is a need to expand cargo-delivery molecules due to the lack of universal delivery tags. Our discovery encouraged us to explore more tags targeting different endocytic receptors for research and therapeutic applications. Moreover, our peptide can provide immediate therapeutic implications. For example, EPP6 is a potential DNA/RNA delivery method due to its ability to bring negatively charged molecules inside the cells. Besides, EPP6 can be applied to target specific cargos due to various receptor expression levels in different tissues/organs.

Finally, EPP6 also demonstrated the potential of monocyclic peptide crossing the blood-brain barrier attributing to its high Papp value.

Even though we consider our studies significant, there remain some limitations that call for future study. For example, the intracellular fate of EPP6 was not fully explored, and more

detailed mechanisms remain unknown. Other than that, the peptide structures can be further modified to identify EPPs with higher penetrating efficacy. In addition, we could further expand the cargo types to enable a more generalized application of our EPPs in the future. Overall, monocyclic peptides are now emerging as a unique class of compounds that offers multifaced uses. Their use in therapeutics has increased significantly over the past few years. Target specificity, better binding affinity, and resistance to hydrolysis-these advantageous features of cyclic peptides make them an excellent choice for targeting complex epitopes for therapeutic, probing, and cargo delivery purposes.